JGR Biogeosciences

RESEARCH ARTICLE
10.1029/2023JG007528

Are Upwelling Systems an Underestimated Source of Long Chain Omega-3 in the Ocean? The Case of the Southern Benguela Upwelling System

Eleonora Puccinelli[1,2,3], Sarah E. Fawcett[3,4], Raquel F. Flynn[3], Jessica M. Burger[3], Gaspard Delebecq[2], Nolwenn Duquesne[2], Christophe Lambert[2], Hazel Little[3], Laure Pecquerie[2], Fany Sardenne[2], Sina Wallschuss[3], and Philippe Soudant[2]

[1]Department of Coastal Systems, Royal Netherlands Institute for Sea Research (NIOZ), Texel, The Netherlands, [2]Laboratory of Environmental Marine Sciences (LEMAR), IUEM, University of Brest, CNRS, IRD, Ifremer, Plouzané, France, [3]Department of Oceanography, University of Cape Town, Cape Town, South Africa, [4]Marine and Antarctic Research Centre for Innovation and Sustainability (MARIS), University of Cape Town, Cape Town, South Africa

Key Points:

- Upwelling promoted phytoplankton long chain omega-3 production which was tightly coupled to the introduction of new nitrate during upwelling
- Pre-upwelling, non-diatom trophic markers were dominant, with a rapid switch over just 2 days to diatom trophic markers post-upwelling
- Long chain omega-3 concentrations were 10 times higher than previous records suggesting that their global production has been underestimated

Supporting Information:

Supporting Information may be found in the online version of this article.

Correspondence to:

E. Puccinelli,
eleonora.puccinelli@nioz.nl

Citation:

Puccinelli, E., Fawcett, S. E., Flynn, R. F., Burger, J. M., Delebecq, G., Duquesne, N., et al. (2023). Are upwelling systems an underestimated source of long chain omega-3 in the ocean? The case of the southern Benguela upwelling system. *Journal of Geophysical Research: Biogeosciences*, *128*, e2023JG007528. https://doi.org/10.1029/2023JG007528

Received 19 APR 2023
Accepted 17 AUG 2023

Author Contributions:

Conceptualization: Eleonora Puccinelli, Sarah E. Fawcett, Fany Sardenne, Philippe Soudant
Data curation: Eleonora Puccinelli, Raquel F. Flynn, Gaspard Delebecq, Nolwenn Duquesne, Christophe Lambert, Hazel Little, Fany Sardenne, Philippe Soudant
Formal analysis: Eleonora Puccinelli, Raquel F. Flynn, Jessica M. Burger, Gaspard Delebecq, Nolwenn Duquesne, Christophe Lambert, Sina Wallschuss, Philippe Soudant

Abstract The Benguela upwelling system (BUS) is one of the world's most productive ecosystems, supporting globally relevant fisheries. The BUS marine community is modulated by the availability of nutrients and omega-3 long chain polyunsaturated fatty acid (hereafter, LC omega-3). Phytoplankton growth in the BUS can be supported by upwelled nitrate, a new nitrogen (N) source to the surface, or by recycled N such as ammonium. Preferential assimilation of one N source over another may yield differences in LC omega-3 production between high and low food-quality species. To evaluate how upwelling and the N source(s) consumed by phytoplankton influence LC omega-3 production, we sampled a BUS anchor station daily for 10 days. Upwelling on days 5–7 supplied high concentrations of nutrients to the surface, while pre- and post-upwelling, surface waters were stratified and nutrient concentrations were low. LC omega-3 and phytoplankton concentrations were near-zero during upwelling, and elevated pre- and post-upwelling. Throughout our sampling, nanoplankton (2.7–10 μm) dominated primary production (30–95%), relying mainly on nitrate to support their growth. Surface LC omega-3 concentrations reached peaks of 215 and 175 μg L^{-1} pre- and post-upwelling, up to 10 times higher than previous measurements from the BUS (<5 μg L^{-1}). Pre-upwelling, non-diatom trophic markers (18:1$n-9$, 18:4$n-3$, 18:5$n-3$) were dominant, with a switch over just two days to diatom trophic markers post-upwelling (16:1$n-7$, 16:2$n-4$, 16:2$n-7$, 16:3$n-4$, 16:4$n-1$). This study reveals the key role of upwelling in promoting phytoplankton LC omega-3 production, which is tightly coupled to the supply of new nitrate. Additionally, the high observed LC omega-3 concentrations suggest that global LC omega-3 production is underestimated.

Plain Language Summary Omega-3 are lipids found in foods such as fish that are extremely important for human health. However, humans and most animals cannot produce omega-3 in sufficient quantities to satisfy their health requirements and must thus acquire them through their diet. In the ocean, the main source of omega-3 is phytoplankton, with different species producing different quantities and kinds of omega-3. Phytoplankton growth also depends on the availability of nutrients, including nitrogen (N). Dominant assimilation of a new N source such as upwelled nitrate versus a recycled N source such as ammonium typically leads to the proliferation of different phytoplankton communities, which may also produce different amounts of omega-3. This study evaluates how upwelling, and the N source(s) used by phytoplankton, influence omega-3 production. During a 10-day investigation conducted off the west coast of South Africa, we found that upwelling promoted phytoplankton omega-3 production and that the community relied mainly on upwelled nitrate. Additionally, community composition changed rapidly during the study in response to upwelling, which was reflected in the amount and kind of omega-3 produced. We observed quantities of omega-3 that were 10 times higher than previous measurements from the region, suggesting that global omega-3 production may be underestimated.

1. Introduction

Omega-3 long chain polyunsaturated fatty acids (PUFA) (≥C_{20}; hereafter, LC omega-3) are essential nutritional compounds for all living organisms including humans, and are sourced predominantly from fish and other seafood (Hicks et al., 2019; Tocher et al., 2019). LC omega-3 have several essential roles, including maintaining

Funding acquisition: Eleonora Puccinelli, Sarah E. Fawcett, Laure Pecquerie, Philippe Soudant
Investigation: Eleonora Puccinelli, Sarah E. Fawcett, Raquel F. Flynn, Jessica M. Burger, Hazel Little, Fany Sardenne
Methodology: Eleonora Puccinelli, Sarah E. Fawcett, Raquel F. Flynn, Jessica M. Burger, Sina Wallschuss
Project Administration: Eleonora Puccinelli
Resources: Eleonora Puccinelli, Sarah E. Fawcett, Laure Pecquerie, Philippe Soudant
Visualization: Eleonora Puccinelli, Raquel F. Flynn, Nolwenn Duquesne, Christophe Lambert
Writing – original draft: Eleonora Puccinelli, Sarah E. Fawcett, Raquel F. Flynn, Jessica M. Burger, Fany Sardenne, Sina Wallschuss, Philippe Soudant
Writing – review & editing: Eleonora Puccinelli, Sarah E. Fawcett, Raquel F. Flynn, Jessica M. Burger, Gaspard Delebecq, Nolwenn Duquesne, Christophe Lambert, Hazel Little, Laure Pecquerie, Fany Sardenne, Sina Wallschuss, Philippe Soudant

membrane function (Parrish, 2013) and enhancing the growth, development, and reproductive output of several organisms (e.g., Garrido et al., 2007; Mourente, 2003; Ravet et al., 2010). Additionally, they constitute a major component of aquaculture feeds (Tacon & Metian, 2009; Tocher, 2015). In the ocean, the main producers of LC omega-3 are phytoplankton, while consumers are unable to synthetize LC omega-3 in sufficient quantities to meet their health requirements, such that they must acquire LC omega-3 through their diet (Arts et al., 2001; Dalsgaard et al., 2003; Litzow et al., 2006). Plankton community composition is the main factor regulating the amount of LC omega-3 produced by a given system (Cañavate, 2019; Galloway & Winder, 2015; Jónasdóttir, 2019). Diatoms, dinoflagellates, and haptophytes are considered high food-quality species, producing high amounts of LC omega-3, in particular eicosapentaenoic-acid (20:5$n-3$, EPA) by diatoms and docosahexaenoic-acid (22:6$n-3$, DHA) by the latter two groups (Dalsgaard et al., 2003; Remize et al., 2020). In contrast, low food-quality species, such as cyanobacteria and chlorophyceae, yield low amounts of LC omega-3 and produce mostly short-chain PUFA (i.e., ≤C18 PUFA; Cañavate, 2019).

The Benguela upwelling system (BUS) off the west coast of southern Africa is one of the four major Eastern Boundary Upwelling Systems (EBUS), which together cover only 2% of global ocean area while accounting for 8% of marine primary production and almost 20% of the global marine fish catch (Pauly & Christensen, 1995). As such, EBUS support many of the world's most important fisheries (e.g., small-pelagic fisheries; Cury & Roy, 1989; Ward et al., 2006). The BUS is divided into two subsystems, the northern BUS and southern BUS (NBUS and SBUS, respectively), which are separated by a permanent upwelling cell located off Lüderitz (Hutchings et al., 2009) and both supports high rates of primary and secondary production (Flynn et al., 2020; Huggett et al., 2009; Shannon, 1985). Upwelling favors phytoplankton production through a succession of known producers of high amounts of LC omega-3, with communities dominated first by diatoms and then by dinoflagellates and/or haptophytes (Burger et al., 2020; Pitcher et al., 1991; Puccinelli, McQuaid, et al., 2016). As such, EBUS may be hot-spot regions for LC omega-3 production.

In EBUS, nitrate (NO_3^-) upwelled from depth is the main nitrogen (N) source fueling primary production (supporting "new production"), with this nutrient estimated to support over 50% of phytoplankton growth on an annual basis (González-Galisteo et al., 2019; Messié et al., 2009; Waldron & Probyn, 1992). The higher-than-average concentrations of iron that are supplied to surface waters by upwelling (Archer & Johnson, 2000; Messié & Chavez, 2015; Patti et al., 2008) lead to the preferential consumption by phytoplankton of upwelled NO_3^- over recycled N (e.g., ammonium (NH_4^+)), with consumption of the latter supporting "regenerated production" (Dugdale & Goering, 1967). NO_3^- assimilation usually promotes the growth of large phytoplankton including diatoms (Fawcett & Ward, 2011; Kudela & Dugdale, 2000), while smaller phytoplankton including cyanobacteria tend to consume NH_4^+ (Fawcett et al., 2011; Probyn & Painting, 1985). It is therefore possible that the assimilation of one N source over another (i.e., NO_3^- over regenerated N), each of which is associated with a different phytoplankton community, will be reflected in LC omega-3 production in a particular system.

Recent studies have indicated that the global supply of LC omega-3 is declining, with current predictions indicating that the supply will soon become insufficient for the growing human population (Colombo et al., 2020; Hixson & Arts, 2016). Indeed, it has been estimated that of the 1.4 Mt annual requirement for EPA + DHA to maintain human population health, only 0.8 Mt are currently available (Hamilton et al., 2020). Moreover, 90% of the global phytoplankton EPA + DHA supply is thought to be lost between primary producers and higher trophic levels (Hamilton et al., 2020). However, information on the LC omega-3 supply from upwelling systems remains scarce (Puccinelli et al., 2021).

With a focus on the SBUS, the broad objective of this work is to improve our knowledge of LC omega-3 production in upwelling systems, including the links to phytoplankton community and N cycle dynamics. Specifically, we hypothesize that (a) low LC omega-3 concentrations before and during upwelling when the system is supported largely by NH_4^+ and a phytoplankton community characterized by non/low producers of LC omega-3 is favored; and (b) high LC omega-3 concentrations post-upwelling due to the proliferation of a phytoplankton community dominated by diatoms, the growth of which is promoted by the uptake of newly upwelled NO_3^-.

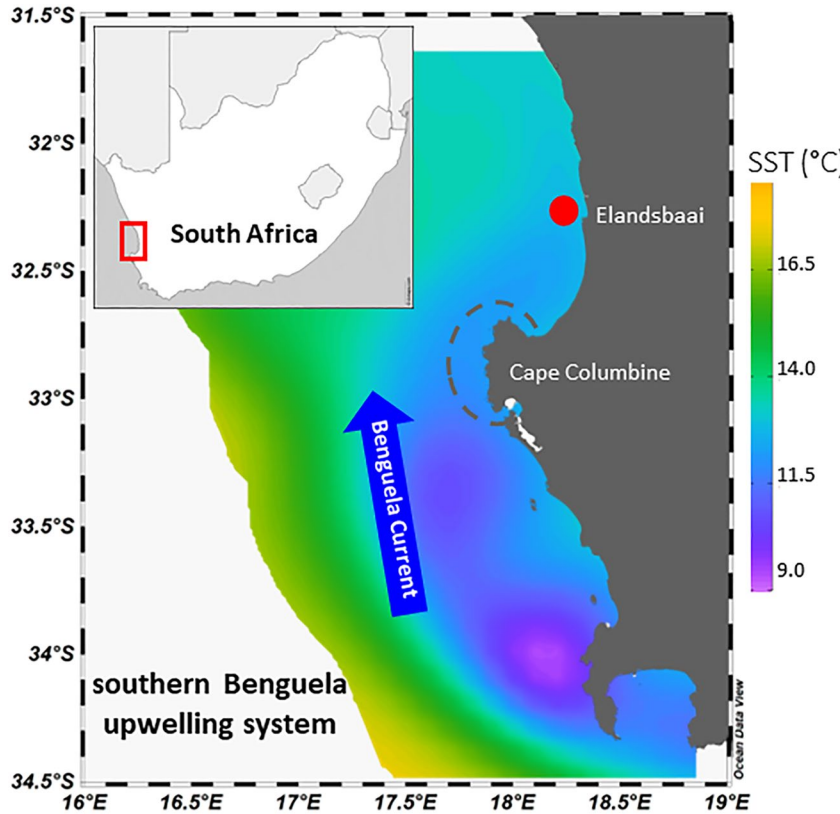

Figure 1. Map of the study area in the southern Benguela upwelling system showing the location of the anchor station in Elandsbaai (red dot) where sampling was conducted. The Cape Columbine upwelling cell is indicated by the gray dotted line. The blue arrow represents the approximate position of the Benguela Current that dominates the surface flow of the SBUS. The current is characterized by two flow paths: the Benguela Oceanic Current and the Benguela Coastal Current (BCC; Veitch et al., 2010) separated by the Oceanic front. BCC is the portion of the current present over the continental shelf that is induced by coastal upwelling (Veitch et al., 2010), which influenced our study site. The colored shading indicates sea surface temperature (SST, °C) on the first day of sampling (11 March 2020) obtained using the Regional Air-Sear Interactions (RASI) tool at the NASA Global Hydrometeorology Resource Center DAAC.

2. Materials and Methods

2.1. Study Area and Sampling Design

Sampling took place aboard the MA-RE1 7.3 m Gemini inflatable craft over 10 consecutive days in late austral summer (11–20 March 2020) during the upwelling season at an anchor station in Elandsbaai in the SBUS (32.308°S; 18.275°E; bottom depth of ∼30 m; Burger et al., 2020) (Figure 1).

Upwelling in the SBUS is wind-driven and occurs seasonally, predominantly during austral summer (Hutchings et al., 2009; Shannon & Nelson, 1996). Wind-driven upwelling events in the vicinity of Cape Columbine (Figure 1) supply cold, nutrient-rich Subantarctic Mode Water (SAMW) and South Atlantic Subtropical Mode Water (SASTMW) to the surface (Flynn et al., 2020; Lamont et al., 2015), which is then advected northwards, including into Elandsbaai (Bailey & Chapman, 1991). Such events result in the mixing of the water column in Elandsbaai and the advection of nutrients into the surface layer.

Wind data from 15 February to 15 April 2020 were used to assess the potential for upwelling events in the sampling region before and after sampling (Table S1). During the 10-day experiment, seawater samples were collected daily using a hand-held 5 L Niskin bottle from seven depths over the water column: surface (0 m), subsurface (5 m), deep (10, 15, 20, 25 m, and bottom ∼30 m), unless otherwise specified. Hydrographic data (temperature and salinity) were generated using a Seabird conductivity-temperature-depth (CTD) profiler. Potential density (σ_θ; kg m^{-3}) was then derived from absolute salinity and conservative temperature with respect to a reference pressure of 0 dbar following IOC (2010). σ_θ was used to calculate the mixed layer depth (MLD; m)

following the de Boyer Montégut et al. (2004) criteria of a change in σ_θ of ≥0.03 kg m^{-3}, but using 0 m as the reference depth given the shallow water depth (~30 m). The diffuse attenuation coefficient of photosynthetically active radiation (Kd(PAR)) was determined from the Secchi disk depth (Idso & Gilbert, 1974; Table S2 in Supporting Information S1) and then used to estimate the depth of the euphotic zone (Zeu, m; Kirk, 1994).

2.2. Sample Collection

Seawater samples were collected for the analysis of oxygen, nutrient- (nitrate, nitrite, ammonium, phosphate, silicic acid) and chlorophyll *a* concentrations, phytoplankton taxonomy and flow cytometry (FC), nitrate isotope ratios, N and carbon (C) stable isotope (SI) ratios of particulate organic matter, rates of net primary productivity (NPP) and N (as NO_3^- and NH_4^+) uptake, and phytoplankton fatty acid composition.

2.2.1. Oxygen and Nutrient Concentrations

Duplicate seawater samples for oxygen analysis were collected in Biological Oxygen Demand (BOD) bottles and immediately fixed and stored in the dark until analysis, which occurred less than 5 hr after sampling. In the laboratory, the dissolved oxygen concentrations were measured using the Winkler titration method (Carpenter, 1965; Grasshoff, 1976).

Nutrients were collected in duplicate 50 mL Falcon tubes and frozen at −20°C until analysis. Nitrate + nitrite and silicic acid concentrations ($[(NO_3^- + NO_2^-)]$ and $[Si(OH)_4]$) were measured using a Lachat QuickChem flow injection analysis platform (Diamond, 1994; Grasshoff, 1976). The detection limit for both nutrients was 0.1 µM. Phosphate and nitrite concentrations ($[PO_4^{3-}]$ and $[NO_2^-]$) were measured manually using standard colorimetric methods (Parsons et al., 1984), with a detection limit of 0.05 µM. The NO_3^- concentrations were calculated by subtracting $[NO_2^-]$ from $[NO_3^- + NO_2^-]$. Aliquots of a certified reference material (CRM; JAMSTEC; Lot CG) were analyzed during auto-analyzer and manual runs to ensure measurement accuracy. The fluorometric method (Holmes et al., 1999) was used to analyze the NH_4^+ concentrations ($[NH_4^+]$), with a detection limit of 0.05 µM. The $[NH_4^+]$ measurements were corrected for the matrix effect (ME) (Saxberg & Kowalski, 1979).

2.2.2. Chlorophyll *a* and Phytoplankton Taxonomy

Seawater (1 L from each depth) was collected in opaque high-density polyethylene bottles for chlorophyll *a* analysis. From each depth, 300 mL of seawater was filtered through a combusted (all glass fiber filters (GF/F) were combusted at 450°C for 5 hr) 0.3 µm GF/F, 300 mL through a 2.7 µm GF/F, and the remaining 400 mL through a 10 µm nylon mesh for the determination of chlorophyll *a* concentrations of different phytoplankton size classes (picoplankton: 0.3–2.7 µm; nanoplankton: 2.7–10 µm; microplankton: >10 µm). The chlorophyll *a* on each filter was extracted in 90% acetone for 24 hr at −20°C in the dark, after which fluorescence was determined following Welschmeyer (1994). The chlorophyll *a* concentrations ([Chl *a*]) of the picoplankton and nanoplankton were then determined by subtraction: $[\text{Chl } a]_{\text{picoplankton}}$ = [Chl *a*] on the 0.3 µm filter − [Chl *a*] on the 2.7 µm filter; $[\text{Chl } a]_{\text{nanoplankton}}$ = [Chl *a*] on the 2.7 µm filter − [Chl *a*] on the 10 µm filter. The microplankton [Chl *a*] was taken to be the [Chl *a*] on the 10 µm filter.

Two approaches were used to investigate phytoplankton community composition. For identification and enumeration of larger phytoplankton, samples were collected using a plankton net (50-µm mesh size and 25-cm diameter) deployed vertically to 5 m (total volume of water filtered ~245 L). The contents were transferred to a Falcon tube and immediately fixed with 200 µL of a 25% glutaraldehyde solution. Phytoplankton were enumerated from subsamples using an inverted microscope (640× magnification), with identification to the highest taxonomic level possible.

For identification and enumeration of the smaller phytoplankton community, triplicate seawater samples (2 mL) were collected in cryovials and immediately fixed with 20 µL of a glutaraldehyde solution (glutaraldehyde 0.3% final concentration) for FC, then frozen at −80°C until analysis. The following phytoplankton groups were identified and counted: FC-picoplankton (~0.5–<3 µm), FC-nanoplankton (~2–20 µm), *Synechococcus*-like cells (~1–3 µm), and cryptophyte-like cells (~10–30 µm). Green-fluorescent polystyrene bead solution ("Flow Check," Polyscience, 1% in sterile 0.2 µm filtered seawater) was used as the internal standard. The biovolume of each group was calculated following Bouvier et al. (2001).

2.2.3. Nitrate Isotopes

The N and oxygen (O) isotope ratios of seawater nitrate ($\delta^{15}N_{NO3}$ and $\delta^{18}O_{NO3}$; where $\delta^{15}N$, in ‰ versus N_2 in air, = $[(^{15}N/^{14}N)_{\text{sample}}/(^{15}N/^{14}N)_{\text{ref}} - 1] \times 1{,}000$ and $\delta^{18}O$, in ‰ versus VSMOW, = $[(^{18}O/^{16}O)_{\text{sample}}/$

$(^{18}O/^{16}O)_{ref} - 1] \times 1{,}000))$ were measured using the denitrifier method (Casciotti et al., 2002; Sigman et al., 2001) and a Delta V Advantage isotope ratio mass spectrometer (IRMS). Prior to isotopic analysis, samples were treated with sulfamic acid to remove NO_2^- (Fawcett et al., 2015; Granger & Sigman, 2009). Results were referenced to atmospheric N_2 and VSMOW using the CRMs, IAEA-NO-3 ($\delta^{15}N = 4.7 \pm 0.2‰$; Gonfiantini et al., 1995 and $\delta^{18}O = 25.6 \pm 0.4‰$; Böhlke et al., 2003) and USGS-34 ($\delta^{15}N = -1.8 \pm 0.1‰$ and $\delta^{18}O = -27.9 \pm 0.3‰$; Böhlke et al., 2003). The analytical precision for repeat $\delta^{15}N_{NO3}$ and $\delta^{18}O_{NO3}$ measurements was ≤0.1‰ and ≤0.2‰, respectively.

2.2.4. Particulate Organic Matter

Seawater (1L from each depth) was collected in opaque high-density polyethylene bottles for particulate organic N (PON) and carbon (POC) analysis following prefiltration through a 200-µm mesh to remove large grazers. At each depth, as per the chlorophyll *a* analyses, 300 mL of seawater was filtered through a 0.3 µm GF/F, 300 mL through a 2.7 µm GF/F, and the remaining 400 mL through a 10 µm nylon mesh. The material on the 10 µm nylon mesh was resuspended in filtered seawater (<0.2 µm), then collected on a 0.3 µm GF/F. Filters were stored in combusted foil at −20°C pending analysis.

In the laboratory, filters were oven-dried at 40°C for 24 hr and pelletized in tin capsules. Samples were analyzed for PON and POC content and $\delta^{15}N$ and $\delta^{13}C$ ($\delta^{13}C$, in ‰ versus VPDB, $= [(^{13}C/^{12}C)_{sample}/(^{13}C/^{12}C)_{ref} - 1] \times 1{,}000$) using a Flash Elemental Analyzer 1112 Series coupled to a Delta V Plus IRMS. A protocol blank (unused precombusted filter + tin capsule) was run after every 10–20 samples and laboratory standards calibrated to IAEA CRMs were run after every five samples. The detection limit was 2 µg C and 1 µg N, and analytical precision was <0.1‰ for $\delta^{13}C$ and $\delta^{15}N$. The PON and POC of the picoplankton and nanoplankton size classes were calculated by subtraction as for chlorophyll *a*. Their $\delta^{15}N$ and $\delta^{13}C$ values were then calculated, accounting for the concentration of PON and POC in each size class: $\delta^{15}N$ or $\delta^{13}C$ picoplankton = [($\delta^{15}N$ or $\delta^{13}C$ × PON or POC on the 0.3 µm filter) − ($\delta^{15}N$ or $\delta^{13}C$ × PON or POC on the 2.7 µm filter)]/(PON or POC on the 0.3 µm filter − PON or POC on the 2.7 µm filter); $\delta^{15}N$ or $\delta^{13}C$ nanoplankton − [($\delta^{15}N$ or $\delta^{13}C$ × PON or POC 2.7 µm filter) − ($\delta^{15}N$ or $\delta^{13}C$ × PON or POC 10 µm filter)]/(PON or POC 2.7 µm filter − PON or POC 10 µm filter). The $\delta^{15}N$ or $\delta^{13}C$ of microplankton (>10 µm) was represented by the measured $\delta^{15}N$ or $\delta^{13}C$ of the 10 µm filter.

2.2.5. Rates of NPP and N Uptake

Daily simulated in situ experiments were conducted to determine the rates (µM hr^{-1}) of C fixation (NPP) and N uptake (as NO_3^- and NH_4^+; ρNO_3^- and ρNH_4^+) at five depths: 0, 5, 10, 15, and 20 m. At each depth, seawater was prefiltered (200 µm) into four 1 L clear polycarbonate bottles. Two bottles (duplicates) were amended with $K^{15}NO_3$ and $NaH^{13}CO_3$ (final ^{15}N and ^{13}C concentration of 0.5 and 100 µM, respectively) and two bottles with $^{15}NH_4Cl$ (final ^{15}N concentration of 0.05 µM). Bottles were incubated in situ for 4 hr by attaching them to an anchored rope, with each bottle fastened at its depth of collection. Experiments were terminated via filtration of the 1 L bottle contents: 300 mL through a 0.3 µm GF/F, 300 mL through a 2.7 µm GF/F, and 400 mL through a 10 µm nylon mesh. The material on the 10 µm nylon mesh was resuspended in filtered seawater (<0.2 µm), then collected on a 0.3 µm GF/F. Filters were stored in combusted foil at −20°C until analysis. The incubation filters were analyzed for PON and POC content and N and C isotopes as described for the PON and POC samples. NPP, ρNO_3^-, and ρNH_4^+ were then calculated following Dugdale and Wilkerson (1986):

$$\rho_x = \left(\frac{(R_{xs})}{((R_{enr}) - (F)) \times T} \right) \times \text{PON or POC} \quad (1)$$

where x is C, NH_4^+, or NO_3^-; R_{xs} is the measured ^{15}N or ^{13}C atom % in the PON or POC minus the natural abundance atom % (F, = 0.366% for ^{15}N and 1.07% for ^{13}C), R_{enr} is the atom % of ^{15}N or ^{13}C in the incubation seawater directly following tracer addition (calculated for ^{15}N using the measured NH_4^+ and NO_3^- concentrations and assumed for ^{13}C to be 5%), and T is the incubation length (hr). The rates of NPP, ρNO_3^-, and ρNH_4^+ associated with the picoplankton and nanoplankton were calculated by subtraction as for the chlorophyll *a*, PON and POC, with the microplankton rates determined from the 10 µm filter measurements.

2.2.6. Fatty Acids

Seawater (4 L) for FA analysis was prefiltered (200 µm) and collected in triplicate from four depths: 0, 5, 10, and 30 m. The seawater was filtered through a 0.3 µm GF/F, then immediately stored in liquid nitrogen and subsequently at −80°C until analysis. Samples were lyophilized for 48 hr upon arrival in the laboratory.

Lipids were extracted using a modification of the Folch et al. (1957) procedure through homogenization in 6 mL of a fresh solution of methanol and chloroform (2/1; v/v) and closed under N_2 atmosphere. FA methyl esters (FAME) were obtained after acidic transesterification by the addition of a H_2SO_4/methanol solution (3.4%; v/v) and heating at 100°C for 10 min. FAME composition was determined using a Varian CP8400 Gas Chromatograph equipped with a ZBWAX column with hydrogen as the carrier gas. Peaks were identified by comparison with retention times of external standards (Supelco37, PUFA No. 1 and No. 3, Bacterial Acid Methyl Ester Mix; Sigma). FAME peak area was converted into µg of FA based on the peak area of the internal standard (23:0). FA are reported using the notation $A{:}Bn-x$, where A is the number of carbon atoms, B is the number of double bonds, and x indicates the position of the first double bond relative to the terminal methyl group (Puccinelli, McQuaid, et al., 2016). Among the common FA trophic markers (TM), LC omega-3 constitutes the sum of long chain ($\geq C_{20}$) $n-3$, including 20:3$n-3$, 20:4$n-3$, 20:5$n-3$, 21:5$n-3$, 22:5$n-3$, and 22:6$n-3$. The sum of 16:1$n-7$, 16:2$n-4$, 16:2$n-7$, 16:3$n-4$, 16:4$n-1$ was used as a diatom TM and the sum of 18:1$n-9$, 18:4$n-3$, 18:5$n-3$ as a non-diatom TM (i.e., haptophyte and dinoflagellate; Parrish et al., 2000). The ratio of EPA/DHA was used to identify communities mostly supported by non-diatoms (ratio <1) or by diatoms (ratio >1) (Dalsgaard et al., 2003). Additionally, the nutritional quality of phytoplankton for higher trophic levels was estimated using the FA-based nutritional quality index (NQI) calculated following Equation 1 of Cañavate (2019).

2.3. Data Analysis

A multivariate permutational analysis (PERMANOVA; Anderson et al., 2008) was performed to test for differences in the phytoplankton FA composition with depth ($n=4$) and day ($n=10$). Canonical analyses of principal coordinates (CAP) were used to explore differences in the phytoplankton FA composition between *Depth* and *Day*, focusing on the 0 and 5 m samples where most of the FA were recorded. FA analyses were based on Euclidian dissimilarities calculated from percentage data. Only FA that contributed >1% to the total FA (TFA) were included in the analyses. The analyses were conducted using the PERMANOVA + add-on package of PRIMER v6 (Anderson et al., 2008). No statistical analyses were performed on the other data. PRIMER v6, SigmaPlot, Ocean Data View (OVD), and R software were used for visualization of the data.

3. Results

3.1. Hydrography

The upper water column (upper ~5–10 m) was well-stratified over much of the sampling period, except on days 5, 6, and 7 when an upwelling event occurred. During these 3 days, a decrease in temperature, density, oxygen, and chlorophyll *a* concentrations was observed, coincident with an increase in the NO_3^- concentration (Figures 2, 3a, and 4a–4c). Pre- and post-upwelling, surface temperature (0 m) was >17°C, dropping as low as 13°C during upwelling, while oxygen concentrations decreased from 360 µM pre-upwelling to a minimum of 220 µM during upwelling (Table S3).

The wind direction during the 10-day investigation was variable; however, south-south-westerly winds were the most prevalent. These winds were also prevalent for the months prior to and after the study period (Table S1). Wind speed was significantly higher on days 5, 6, and 9 (4.9, 3.6, and 3.6 m s^{-1}, respectively) than on the other days (<3 m s^{-1}). Additionally, high wind speeds were recorded 12 and 3 days prior to the study period (6.1 and 4.1 m s^{-1}, respectively).

3.2. Nutrient Concentrations

The nutrient profiles followed the same temporal pattern as the physical parameters (Figure 2, Figure S1 in Supporting Information S1 and Table S3). Pre- and post-upwelling, most nutrient concentrations were higher below the mixed layer (>5–10 m), with [NO_3^-] and [$Si(OH)_4$] as high as 27.9 and 30.0 µM, and [PO_4^{3-}] and [NO_2^-] reaching 3.0 and 1.4 µM, respectively. During the upwelling period, mixed-layer nutrient concentrations were elevated, with the highest surface concentrations measured on day 7, of 14.9 µM (NO_3^-), 13.1 µM (SiO_4^-), 3.0 µM (PO_4^{3-}), and 1.5 µM (NO_2^-). The [NH_4^+] showed a different trend from the other nutrients. While [NH_4^+] was generally low (<2 µM) throughout the study, water-column concentrations were higher during the

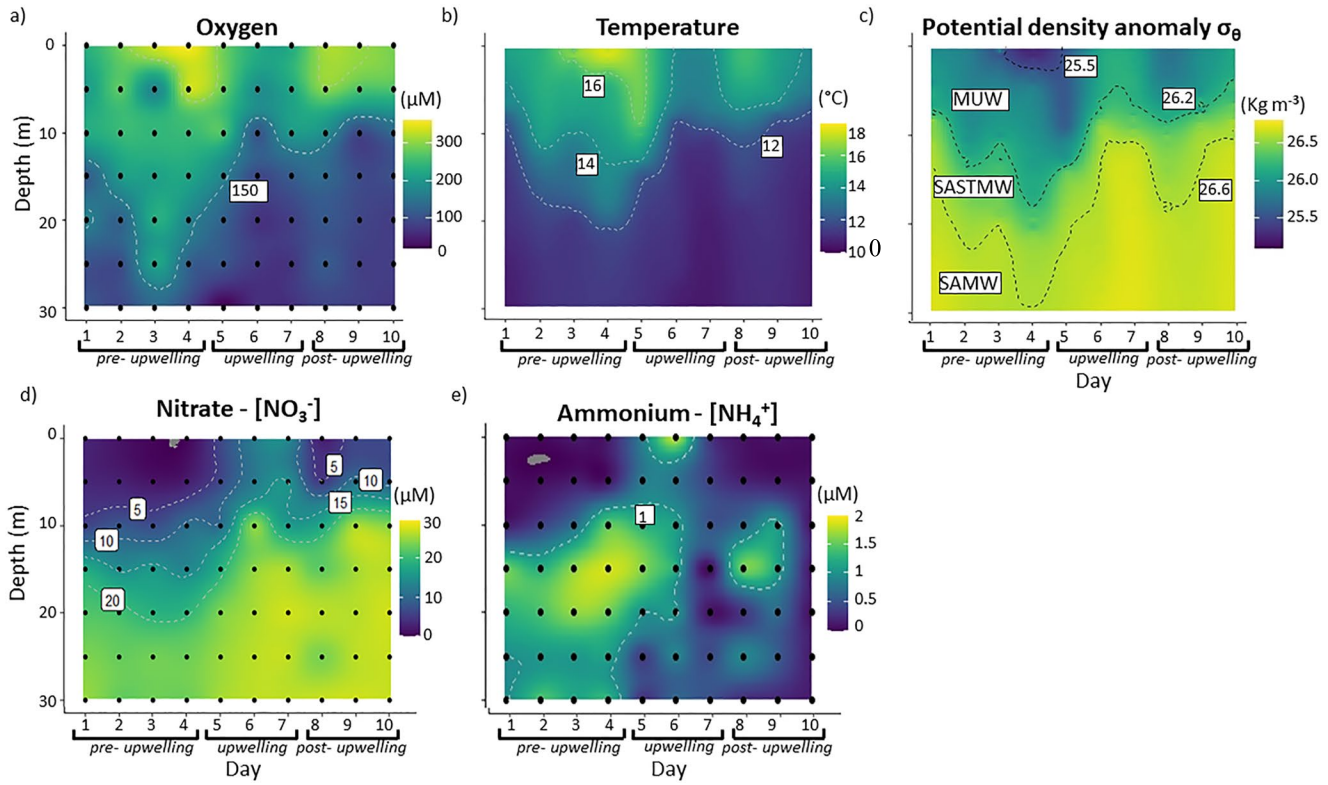

Figure 2. Vertical profiles of (a) oxygen concentration, (b) temperature, (c) the potential density anomaly (σ_θ), (d) nitrate (NO_3^-), and (e) ammonium (NH_4^+) concentrations sampled over 10 consecutive days at the anchor station in the southern Benguela upwelling system in March 2020. The black dots in panels a, d, and e show the discrete sampling depths. The dashed black lines in panel c indicate the isopycnals separating the main water masses present in the study region: Subantarctic Mode Water (SAMW), South Atlantic Subtropical Mode Water (SASTMW), and Modified Upwelled Water (MUW).

non-upwelling period (maximum of 1.9 µM at 20 m on day 4). Maximum surface (<5 m) [NH_4^+] was measured during upwelling on day 6 (1.8 µM), while the lowest values were measured on days 7 and 10 (<0.1 µM).

3.3. Chlorophyll *a* and Phytoplankton Community Composition

The chlorophyll *a* concentrations were dominated by the nanoplankton throughout the study, followed by the microplankton and picoplankton (Figures 3a–3c). Nanoplankton contributed the highest chlorophyll *a* concentrations pre- and post-upwelling at 0 and 5 m (5.6 ± 0.3 µg L^{-1}; 68.5 ± 17.4% of total chlorophyll *a*), with nanoplankton chlorophyll *a* decreasing to <2.6 µg L^{-1} during the upwelling event. Microplankton showed low chlorophyll *a* concentrations pre-upwelling and during upwelling (0.9 ± 0.2 µg L^{-1}; 15.0 ± 7.2%), which increased post-upwelling to 3.6 ± 0.3 µg L^{-1} (25.6 ± 10.6%). Picoplankton contributed least to total chlorophyll *a*, with low concentrations throughout the investigation (0.2 ± 0.1 µg L^{-1}; 11.2 ± 5.3%).

Microscopy analyses (phytoplankton >50 µm) indicated differences in phytoplankton abundances in the pre- (4.5 ± 2.2 × 10^4 cell L^{-1}), during (33.8 ± 19.7 × 10^4 cell L^{-1}) and post-upwelling (103.0 ± 63.4 × 10^4 cell L^{-1}) samples, with the highest abundances measured post-upwelling (228.2 × 10^4 cell L^{-1} on day 9). Apart from day 1 when samples contained near-exclusively dinoflagellates (>90% of total cell count), diatoms dominated the phytoplankton assemblage throughout the study period, with *Chaetoceros* spp. and *Pseudo-nitzschia* spp. being the most abundant species (Figure 4 and Table S4a).

FC analyses indicated that heterotrophic bacteria were the most abundant small plankton group (0.5–3 µm) present throughout the investigation, with particularly high abundances pre-upwelling and during upwelling on days 4 and 5 (maximum of 9 × 10^9 cell L^{-1}). *Synechococcus*-like cells were the next most abundant group, particularly on days 2, 3, and 4 (pre-upwelling) between the surface and 10 m (2.4 ± 1.2 × 10^7 cell L^{-1}; 63.9 ± 8.5% of FC cells counted; Figure S2 in Supporting Information S1 and Table S4b). FC-picoplankton,

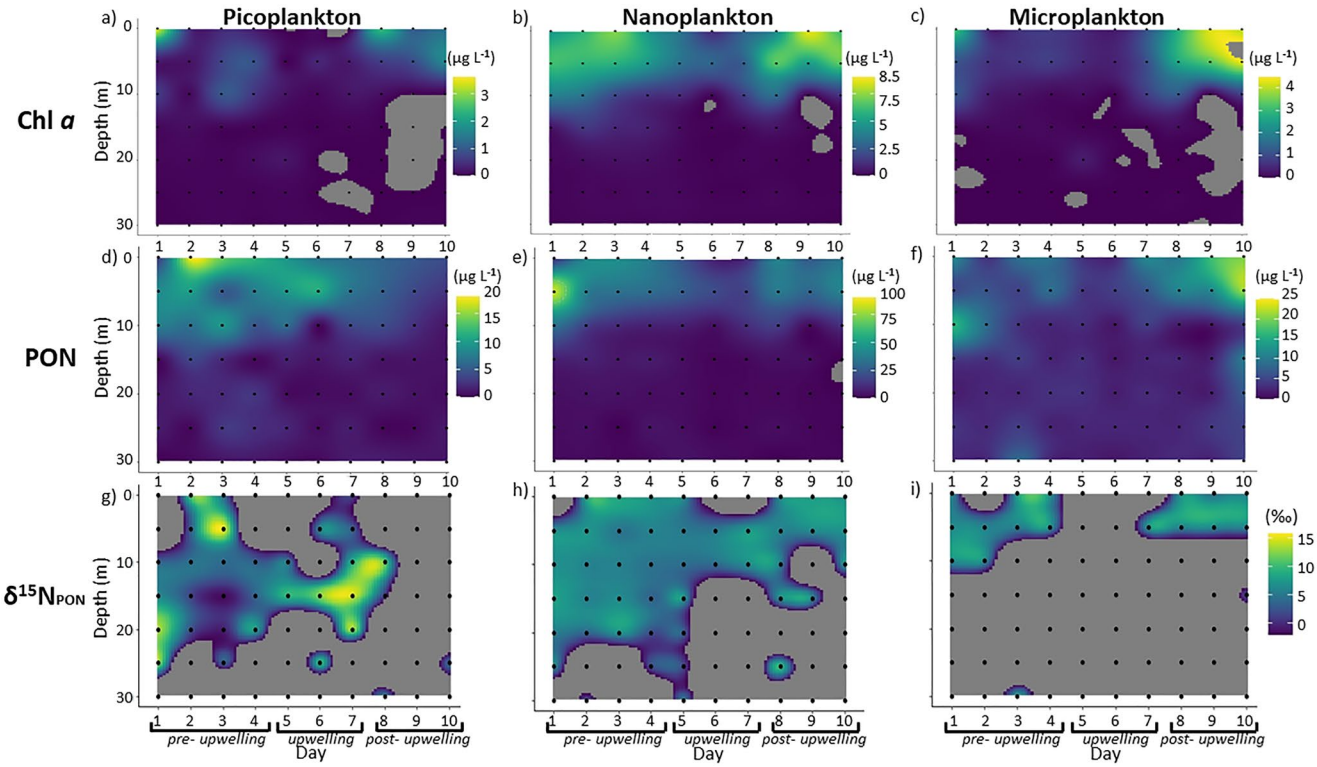

Figure 3. Profiles of picoplankton (0.3–2.7 μm), nanoplankton (2.7–10 μm), and microplankton (>10 μm) (a–c) chlorophyll *a* concentrations, (d–f) particulate organic nitrogen (PON) concentrations, and (g–i) $\delta^{15}N_{PON}$ for samples collected over 10 consecutive days at the anchor station in the southern Benguela upwelling system in March 2020. The gray shading indicates depths and days where concentrations and $\delta^{15}N_{PON}$ were below the methodological detection limits. The black dots indicate discrete sampling depths. Note that the color bar varies from panels a–c and d–f but is the same for panels g–i.

FC-nanoplankton, and cryptophyte-like cells were less abundant (<1.8 × 10^6 cell L^{-1}; <37% of FC cells counted), although FC-nanoplankton were more abundant pre-upwelling compared to during and post-upwelling (1.1 ± 0.5 × 10^6 versus 4.8 ± 2.8 × 10^5 cell L^{-1}; 22.1 ± 8.2 versus 13.0 ± 6.2%). The biovolume was dominated by cryptophyte-like cells pre-upwelling and during upwelling (90% of total FC cell biovolume) and by FC-nanoplankton post-upwelling (99%), with all other groups contributing minimally (Figure S2 in Supporting Information S1 and Table S4b).

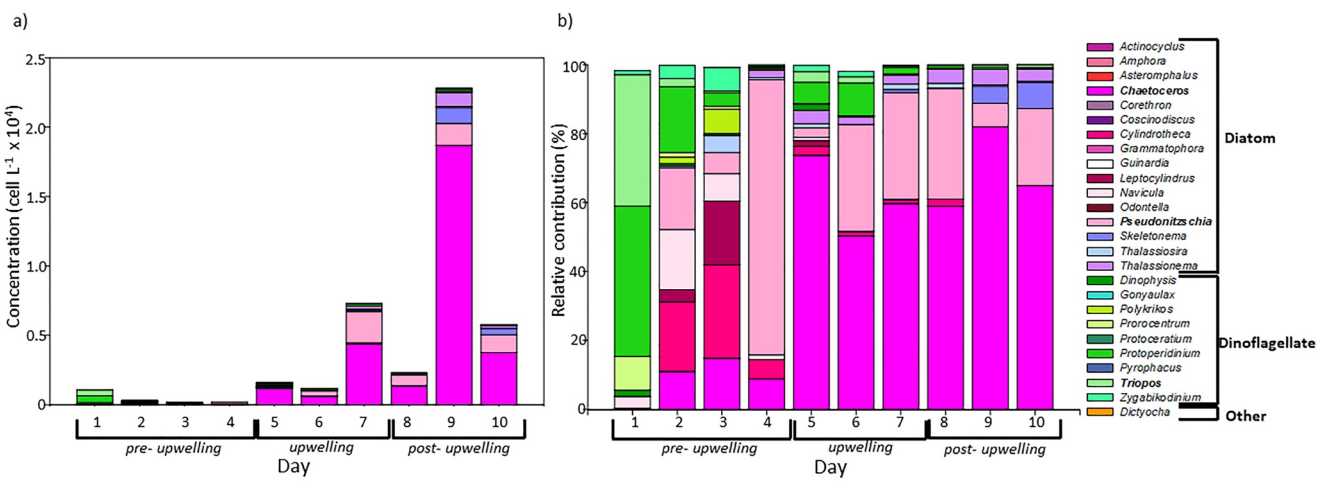

Figure 4. (a) Cell counts (cell L^{-1}) and (b) relative contributions (% of total cells counted) of the different phytoplankton species identified via light microscopy over 10 consecutive days at the anchor station in the southern Benguela upwelling system in March 2020. The most common diatoms (*Chaetoceros* spp., *Pseudo-nitzschia* spp.) and dinoflagellates (*Triopos* spp., *Protoperidinium* spp.) are highlighted in bold in the figure legend.

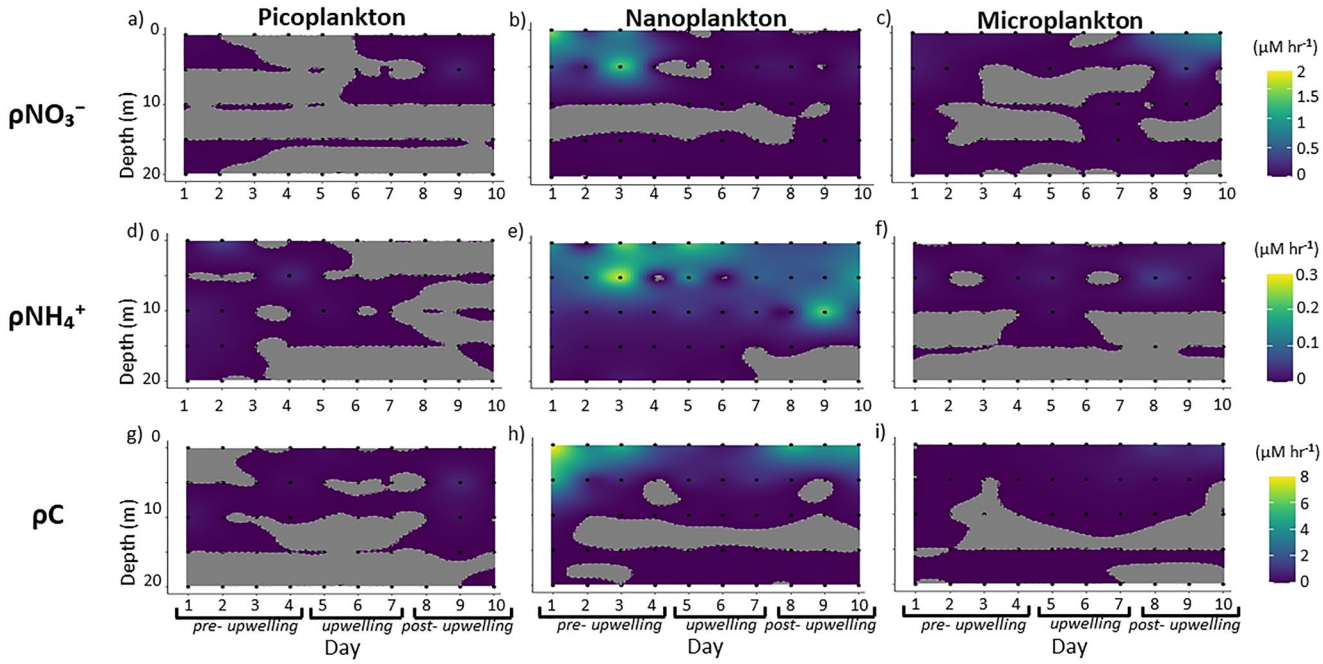

Figure 5. Size-fractionated (picoplankton, 0.3–2.7 μm; nanoplankton, 2.7–10 μm; microplankton, >10 μm) rates of (a–c) nitrate uptake (ρNO_3^-), (d–f) ammonium uptake (ρNH_4^+), and (g–i) net primary production (NPP) measured at five depths (0, 5, 10, 15, and 20 m) over 10 consecutive days at an anchor station in the southern Benguela upwelling system in March 2020. The gray shading indicates depths and days where the rates were below the methodological detection limit.

3.4. Isotope Ratios of Nitrate and Particulate Organic Matter

As for the other parameters, $\delta^{15}N_{NO3}$ was clearly different pre-upwelling, during, and post-upwelling, and varied significantly with depth (Figure S3 in Supporting Information S1 and Table S5). The highest $\delta^{15}N_{NO3}$ was measured at the surface and 5 m pre- and post-upwelling (11.9 ± 2.6‰). At all other depths and at the surface during the upwelling event, the average $\delta^{15}N_{NO3}$ was 7.3 ± 0.9‰. $\delta^{18}O_{NO3}$ followed the same trend, with values of 12.5 ± 3.4‰ observed pre- and post-upwelling at the surface versus 5.8 ± 1.3‰ at depth on all days, as well as at the surface during upwelling.

The majority of the PON was attributed to nanoplankton (up to 91 μg L^{-1}), while microplankton and picoplankton contributed minimally (<25 μg L^{-1} of N; Figures 3d–3f, Table S5). Nanoplankton PON concentrations were particularly high at the surface and subsurface (i.e., 0 and 5 m) pre- and post-upwelling, in contrast to at the other depths and during upwelling (41.9 ± 4.4 versus 6.7 ± 0.1 μg L^{-1} of N). The $\delta^{15}N_{PON}$ of the nanoplankton averaged 6.9 ± 0.3‰ pre- and post-upwelling versus 5.4 ± 0.3‰ during upwelling. The picoplankton PON had a relatively high $\delta^{15}N_{PON}$ at depth during upwelling (maximum of 15‰ on day 7); however, due to the low N content of the samples, for most of the depths and days it was not possible to make reliable $\delta^{15}N_{PON}$ measurements for both the picoplankton and microplankton (Figures 3g–3i).

As for PON, most of the POC was attributed to nanoplankton, with the highest concentrations occurring pre- and post-upwelling at 0 and 5 m (223.3 ± 27.4 versus 41.6 ± 5.5 μg L^{-1} of C; Figure S4 in Supporting Information S1 and Table S5). $\delta^{13}C_{POC}$ varied minimally among the phytoplankton size classes, with microplankton showing slightly lower values than the two other classes (−22.2 ± 1.9‰ versus −19.8 ± 2.7‰). There was no clear effect of upwelling on the $\delta^{13}C_{POC}$.

3.5. Rates of N Uptake and NPP

The highest rates of N uptake and NPP were observed for the nanoplankton size class, while picoplankton and microplankton contributed minimally (ρNO_3^- < 0.9 μM hr^{-1}; ρNH_4^+ < 0.1 μM hr^{-1}; NPP < 1.2 μM hr^{-1}; Figure 5 and Table S6), with their rates in most cases below the methodological detection limit. As such, only the nanoplankton rate data are discussed in detail below (i.e., Figures 5b, 5e, and 5h).

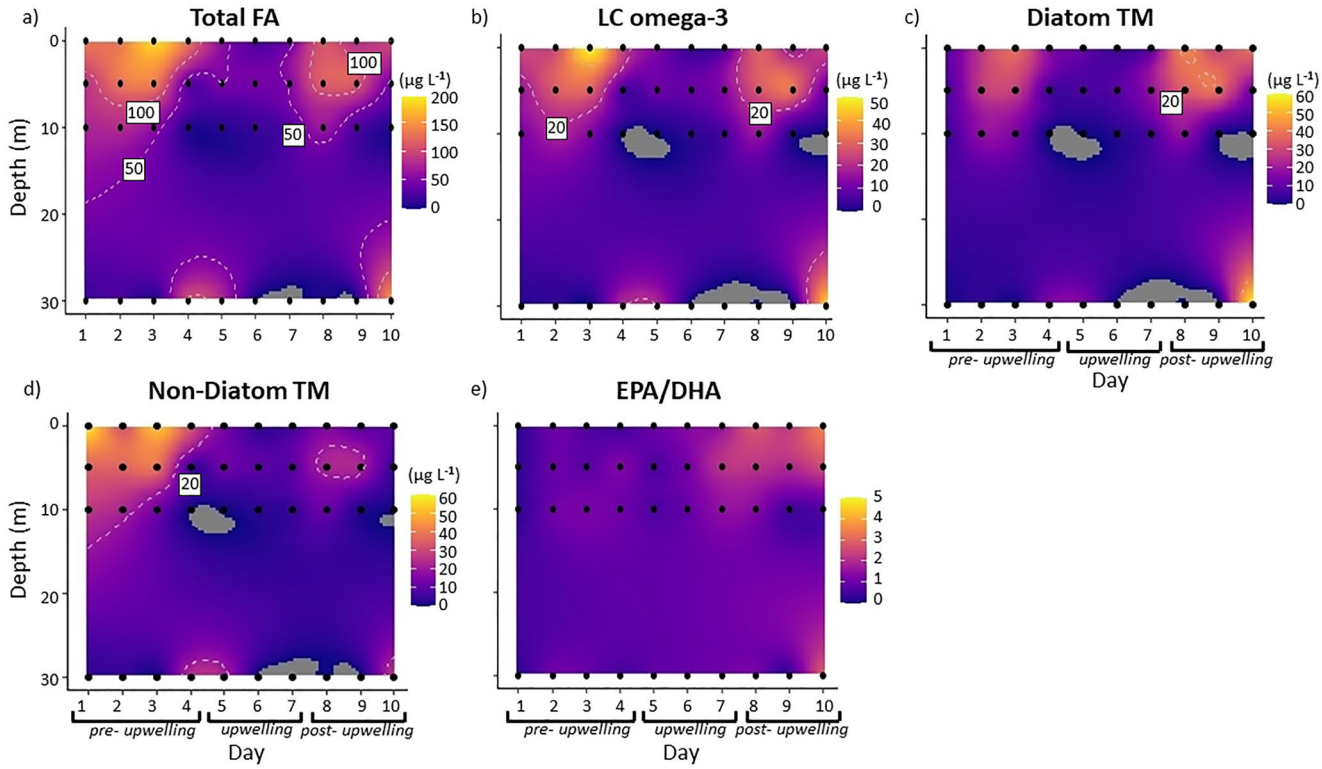

Figure 6. Fatty acid (FA) concentrations (μg L^{-1}) for phytoplankton samples collected from four depths (0, 5, 10, 30 m) over 10 consecutive days at an anchor station in the southern Benguela upwelling system in March 2020. (a) Total FA, (b) LC omega-3 (20:3$n-3$, 20:4$n-3$, 20:5$n-3$, 21:5$n-3$, 22:5$n-3$, 22:6$n-3$), (c) diatom trophic markers (TM; 16:1$n-7$, 16:2$n-4$, 16:2$n-7$, 16:3$n-4$, 16:4$n-1$), (d) non-diatom TM (18:3$n-3$, 18:4$n-3$, 18:5$n-3$), (e) EPA/DHA (20:5$n-3$/22:6$n-3$). The gray shading indicates depths and days where values were below the methodological detection limit.

All the uptake rates varied with depth and were higher pre- and post-upwelling when the water column was strongly stratified, with lower rates measured during active upwelling and when the water column was weakly stratified (Figure 5). Throughout the study, ρNO_3^- was generally higher than ρNH_4^+, with maximum measured rates of 1.7 and 0.3 μM hr^{-1}, respectively (Table S6). ρNO_3^- reached a maximum pre-upwelling in shallow waters (<5 m), especially on day 1 (1.7 μM hr^{-1}) and day 3 (1.4 μM hr^{-1}). Post-upwelling surface and 5 m values of ρNO_3^- were generally low (<0.2 μM hr^{-1}), with rates for the deeper samples and on the other days that were at or below the detection limit (Figure 5b). ρNH_4^+ showed a slightly different pattern from ρNO_3^- in relation to upwelling, with the highest rates measured at 0 m (and in some cases at 5 m) throughout the investigation (0.2 ± 0.1 μM hr^{-1}) except on days 7, 8, and 9 when the surface and 5 m ρNH_4^+ decreased to 0.1 ± 0.0 μM hr^{-1} (Figure 5e). For the other depths and days, ρNH_4^+ was either near or below the detection limit.

NPP was an order of magnitude higher pre- and post-upwelling at 0 and 5 m compared to at depth (>5 m) and on the other days (2.9 ± 0.9 μM hr^{-1} versus 0.2 ± 0.1 μM hr^{-1}). The maximum rate of NPP was recorded at the surface on day 1 (8.0 μM hr^{-1}) followed by surface measurements made on days 3 and 8 (both 5.1 μM hr^{-1}; Figure 5h and Table S6).

3.6. Fatty Acids

The concentrations of phytoplankton TFA showed the same pre- and post-upwelling trends as the other parameters, with values during the upwelling event that were close to 0 μg L^{-1} throughout the water column (Figure 6 and Table S7). TFA concentrations changed with time and depth, and the interaction of time and depth was also significant (PERMANOVA, $p < 0.001$). TFA concentrations were high at 0 and 5 m pre- and post-upwelling, reaching maxima of 185.0 ± 35.4 and 148.0 ± 24.1 μg L^{-1}, respectively. These TFA maxima approximately coincided with peaks in the total POC concentrations, which reached 429 and 240 μg L^{-1} pre- and post-upwelling, respectively, and the two parameters were (weakly) positively correlated (Figure S5 in Supporting

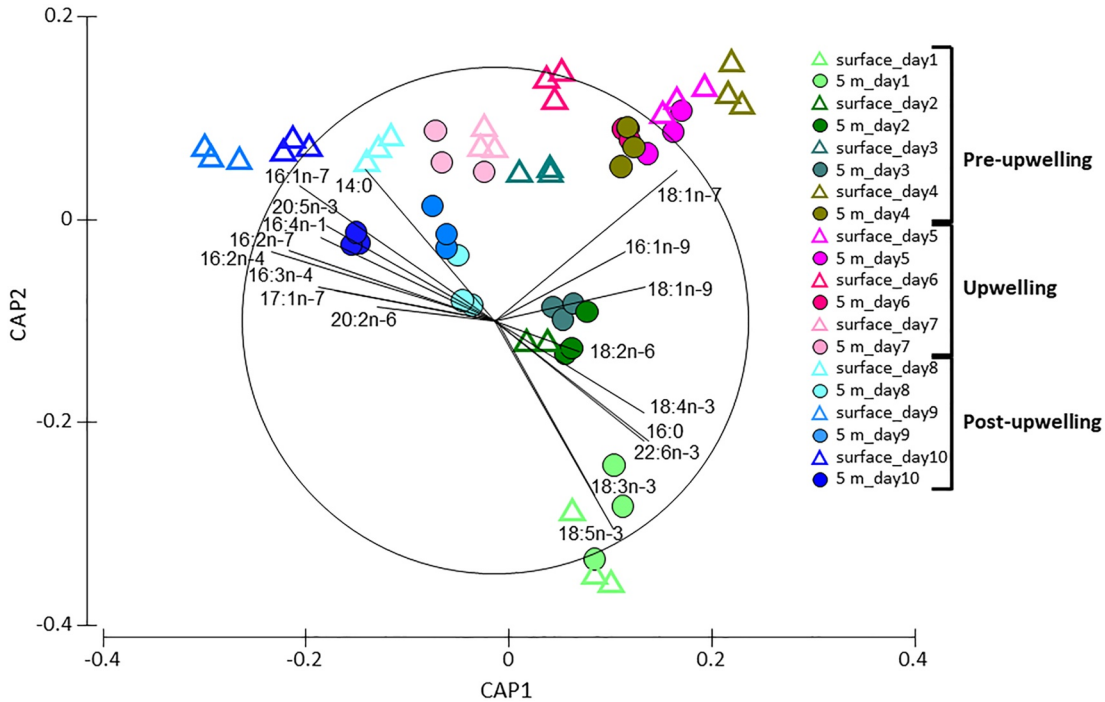

Figure 7. Canonical analysis of principal coordinates (CAP) performed on the fatty acid (FA) composition of phytoplankton samples collected over 10 consecutive days at an anchor station in the southern Benguela upwelling system in March 2020. Only the 0 and 5 m samples were used for the analysis. Color shading indicates different stages of upwelling, as indicated by the environmental data: green = pre-upwelling (days 1–4), pink = during upwelling (days 5–7), blue = post-upwelling (days 8–10). Each symbol represents a single sample. Superimposed is the distribution of eigenvalues for each factor (FA). Only FA that contributed >1% to the TFA were used for the analysis.

Information S1). LC omega-3 followed the same pattern, with the highest concentrations recorded at the surface on day 3 (49.5 ± 6.1 μg L^{-1}, 27% of TFA) and at 5 m on days 8 and 9 (29.3 ± 2.2 μg L^{-1}, 23% of TFA). Most of the TFA sampled pre-upwelling was attributed to non-diatom TM such as ΣC18-PUFA (25.1 ± 4.3 μg L^{-1}, >50% of TFA), particularly 18:5$n-3$, which alone represented up to 20% of the TFA (13.1 ± 4.0 μg L^{-1}, Figures S6 and S7 in Supporting Information S1). By contrast, post-upwelling diatom TM made up as much as 60% of TFA (19.9 ± 0.7 μg L^{-1}) and ΣC16-PUFA constituted 15% of TFA (9.9 ± 1.6 μg L^{-1}). While 18:5$n-3$ was present predominantly pre-upwelling, 18:4$n-3$ was evenly distributed pre- and post-upwelling (Figures S7f and S7g in Supporting Information S1). Peaks of TFA and LC omega-3 were also observed for the deepest samples on days 4, 5, and 10 (TFA of 101.2 ± 6.1, 79.8 ± 1.8, and 148.0 ± 24.2 μg L^{-1}, respectively), with non-diatom TM dominating on days 4 and 5 and diatom TM on day 10 (Figure 6 and Table S7).

The CAP analysis revealed a clear pattern of separation among FA samples collected pre-, during, and post-upwelling, a trend ascribed to non-diatom TM pre-upwelling and diatom TM post-upwelling (Figure 7). The same trend was evident in the EPA/DHA ratio, which was significantly higher post-upwelling, indicating the presence of a phytoplankton community comprising mostly diatoms (values of 0.7 ± 0.1, 1.3 ± 0.1, and 2.5 ± 0.1 for pre-, during, and post-upwelling, respectively; Figure 6e and Table S7).

The NQI based on FA followed the same trend as the other parameters, with higher values at 0 and 5 m pre- and post-upwelling (216.5 ± 15.3) compared to at the other depths and during upwelling (89.7 ± 13.5; Figure 7f and Table S7). The exception to this pattern was the bottom water samples collected on days 4, 5, and 10 for which we derived NQI values of 157.8 ± 23.2, 244.5 ± 10.7, and 297.9 ± 24.8, respectively.

4. Discussion

This study aimed to provide the first estimates of phytoplankton LC omega-3 concentrations for the SBUS and to investigate the potential role of N cycling in influencing LC omega-3 production. As expected, we found that LC omega-3 concentrations were high post-upwelling when diatoms proliferated and when the NO_3^- uptake rates reached a maximum. However, high LC omega-3 concentrations were also observed pre-upwelling, in contrast to

the expectation to find a community producing low amount of LC omega-3. Also surprising was the observation that the LC omega-3 concentrations were much higher (~10 times) than estimates currently available for the SBUS (Puccinelli et al., 2021). Below, we explore possible explanations for the upwelling related patterns that we observed and discuss the implications for LC omega-3 availability to higher trophic levels.

4.1. Upwelling Events and the N Sources Available to Phytoplankton

During the 10-day investigation, we recorded an upwelling event on days 5, 6, and 7, which drove a decrease in the mixed-layer temperature and oxygen concentration coincident with an increase in the nutrient concentrations (Figure 2). This phase occurred between pre-upwelling (days 1–4) and post-upwelling (days 8–10) periods that were associated with a well-stratified upper (~5 m) water column and a shallow mixed layer, consistent with expectations for the SBUS during periods of relaxation (Aristizábal et al., 2017; Bailey & Chapman, 1991; Burger et al., 2020; Zhang et al., 2015). During the non-upwelling periods, NPP and chlorophyll *a* reached a maximum at 0 and 5 m (Figure 3), facilitated by favorable conditions for phytoplankton growth, including high nutrient and light availability. The values recorded here (54.1 ± 12.1 μM d^{-1} and 6.8 ± 3.5 μg L^{-1} for NPP and chlorophyll *a*, respectively) are similar to previous observations made in Elandsbaai in summer (45 μM d^{-1} and 9–15 μg L^{-1}; Burger et al., 2020; Pitcher et al., 1991), with elevated phytoplankton productivity generally occurring immediately following the cessation of upwelling (i.e., at the onset of relaxation), highlighting the pivotal role of the upwelling cycle in modulating productivity in this region.

The two main N sources in the system, NO_3^- and NH_4^+, were delivered to surface waters during upwelling, yielding a surface [NO_3^-] that was twofold higher than the [NH_4^+] (Figure 2 and Table S3). Elevated [NO_3^-] is typically supplied to the surface by the upwelling of SAMW, the ultimate source of nutrients to the SBUS (Flynn et al., 2020; Lamont et al., 2015). Additionally, in shallow regions of the SBUS such as Elandsbaai (maximum depth of 30 m), nutrients (including NO_3^-) tend to accumulate in bottom waters following periods of biomass production as a result of upper water-column stratification, high rates of remineralization, and water-mass retention (i.e., "nutrient trapping"; Flynn et al., 2020); these nutrients are then supplied to the surface layer when upwelling and/or wind-driven mixing ventilates the bottom waters. The higher [NH_4^+] at the surface during the upwelling period can also be explained by water column mixing given that [NH_4^+] was elevated at depth (1.5–2.0 μM at >15 m) during much of our investigation. By contrast, [NH_4^+] was extremely low in surface waters pre- and post-upwelling, presumably due to rapid NH_4^+ uptake by phytoplankton (Dortch, 1990) and the fact that shallow stratification prevented the upward supply of deep NH_4^+. The high [NH_4^+] at depth can be explained by NH_4^+ production in excess of its consumption during organic matter decomposition (i.e., heterotrophic NH_4^+ production in excess of NH_4^+ oxidation), as well as NH_4^+ efflux from the sediments following organic matter remineralization (Burger et al., 2020; Dugdale et al., 2006; Flynn et al., 2020).

While NH_4^+ should theoretically be the preferred N source to phytoplankton given its low oxidation state (−3), which makes its assimilation energetically favorable (Dortch, 1990), its euphotic zone concentration was too low (on average <<1 μM) to support the rates of productivity observed in Elandsbaai. In contrast, high ρNO_3^- are commonly recorded for phytoplankton in upwelling regions, especially when diatom-dominated (Bode et al., 1997; Fawcett & Ward, 2011; Glover et al., 2007). In Elandsbaai, the rapid increase in ρNO_3^- within just 2 days of upwelling, and the coincident decline in surface NO_3^-, $Si(OH)_4$, and PO_4^{3-} concentrations (Figure 5 and Figure S1 in Supporting Information S1), is typical of the response of diatoms to a nutrient supply event (Fawcett & Ward, 2011; Kudela & Dugdale, 2000). Diatoms are able to increase both their nutrient uptake and growth rates very quickly, which allows them to consume a disproportionate fraction of the newly available nutrients and outpace their grazers (Burger et al., 2020; Fawcett & Ward, 2011; Van Oostende et al., 2015). Diatoms can also accumulate excess NO_3^- intracellularly to use when nutrients become depleted (Kudela & Dugdale, 2000). Combined, these strategies allow diatoms to dominate the biomass following upwelling. Our microscopy data are consistent with this idea, indicating a general dominance of diatoms throughout the investigation, which strengthened post-upwelling (Figure 4), thereby confirming our expectation of increased diatom abundance post-upwelling event.

Regardless of the parameters investigated (N uptake rates, NPP, chlorophyll *a*, PON, POC), most of the production in the system was associated with the nanoplankton. Nanoplankton dominance has previously been observed for this system, and in other upwelling regions with similar features to the SBUS (Bode et al., 1997; Burger et al., 2020; Probyn, 1992). It has been suggested that this group can thrive in such systems because of their

intermediate size, being large enough to avoid predation but small enough to remain in the euphotic zone during periods of relaxation, which exposes them to high nutrient- and light availability (Burger et al., 2020). Smaller cells are also less susceptible to light limitation (Finkel, 2001) and have a high affinity for nutrients, resulting in a rapid growth rate (Litchman, 2007).

The dominance of the nanoplankton size class was at least partially reflected in the FC data, which show that cryptophyte-like cells (<30 μm) followed by FC-nanoplankton contributed most to FC biovolume (Figure S2 in Supporting Information S1). In contrast, the microscopy data indicate a general higher contribution of large diatoms (>50 μm) throughout the investigation (except on day 1), particularly the chain-forming *Chaetoceros* spp., with abundances progressively increasing post-upwelling. The two techniques record different phytoplankton size ranges, with microscopy conducted on samples collected in a 50-μm mesh net, while the maximum cell size that the flow cytometers could analyze was 30 μm. Nonetheless, the results of both techniques support the idea of a dominant role for nanoplankton. *Chaetoceros* spp. can exist as single cells (typically of ∼10 μm) or as chains, and thus could have been present in both the FC and microscopy samples. *Chaetoceros* spp. has been shown to dominate the biomass and productivity of Elandsbaai during mid-summer upwelling, which has been attributed to the ability of their group to leverage the advantages of being both relatively small (nanoplankton-sized single cells) and large (once aggregated as chains) (Burger et al., 2020). It is likely that similar dynamics were ongoing during our late-summer investigation.

The $\delta^{15}N_{NO3}$ and $\delta^{18}O_{NO3}$ were high at 0 and 5 m pre- and post-upwelling and consistently lower (>5‰ difference) at depth and throughout the water column during upwelling (Figure S3 in Supporting Information S1). The deep $\delta^{15}N_{NO3}$ of 7.3 ± 0.9‰ is slightly higher than the $\delta^{15}N_{NO3}$ of SAMW, the ultimate source water to the SBUS ($\delta^{15}N_{NO3}$ = 6.6 ± 0.2‰), and similar to that of SASTMW ($\delta^{15}N_{NO3}$ = 7.2 ± 0.3‰), which derives from SAMW and can also upwell in the SBUS (Flynn et al., 2020). The high $\delta^{15}N_{NO3}$ in surface waters (11.9 ± 2.6‰) is indicative of photosynthetic NO_3^- assimilation as phytoplankton preferentially consume ^{14}N-bearing NO_3^-, leaving the residual NO_3^- pool enriched in ^{15}N (Mariotti et al., 1981; Sigman et al., 1999). The coincident rise in $\delta^{18}O_{NO3}$ in shallow waters (Figure S3 in Supporting Information S1) is consistent with this interpretation as NO_3^- assimilation causes $\delta^{15}N_{NO3}$ and $\delta^{18}O_{NO3}$ to increase in unison (Granger et al., 2010). In contrast, the decline in $\delta^{18}O_{NO3}$ at depth that coincides with almost no change in $\delta^{15}N_{NO3}$ (Figure S3 in Supporting Information S1) is characteristic of nitrification (i.e., NO_3^- regeneration; Flynn et al., 2020). During nitrification, the $\delta^{15}N_{NO3}$ of the produced NO_3^- is set by the $\delta^{15}N_{NO3}$ of the organic matter being remineralized (itself set by the N sources consumed by phytoplankton), while its $\delta^{18}O_{NO3}$ is set by that of water ($\delta^{18}O_{NO3}$ of ∼0‰) plus an isotopic offset of ∼1‰ (Boshers et al., 2019; Buchwald et al., 2012; Sigman et al., 2009). The $\delta^{15}N_{NO3}$ and $\delta^{18}O_{NO3}$ observed at depth and during upwelling could also have been influenced by coupled nitrification-denitrification at the sediment-water interface (i.e., benthic-pelagic coupling; Figure S3 in Supporting Information S1). This pathway drives a loss of low-$\delta^{15}N$ N (as N_2 gas), which raises the $\delta^{15}N$ of the remaining NO_3^- pool while coincidentally decreasing its $\delta^{18}O_{NO3}$ (Flynn et al., 2020; Granger et al., 2011). It is difficult to characterize the extent to which coupled nitrification-denitrification may have been ongoing in Elandsbaai at the time of our sampling given that the $\delta^{15}N_{NO3}$ of the deepest samples (25 and 30 m) was ∼6.6–6.9‰, which is very similar to that of SAMW (Flynn et al., 2020). Regardless, the NO_3^- isotope data point to rapid NO_3^- regeneration at depth, which yields high concentrations of recycled nutrients that, once supplied to the surface during mixing, can augment the off-shelf (i.e., SAMW and SASTMW) nutrient supply, enhancing SBUS productivity (Bailey, 1991; Flynn et al., 2020; Tyrrell & Lucas, 2002). One consequence of these dynamics, however, is a decline in bottom-water oxygen concentrations, often to hypoxic levels (Flynn et al., 2020; Monteiro et al., 2011; Pitcher & Calder, 2000).

Preferential phytoplankton consumption of NO_3^- over NH_4^+ was not only evident in the ρNO_3^-, but also in the $\delta^{15}N_{PON}$ of nanoplankton. This group had a $\delta^{15}N_{PON}$ in the surface layer that was ∼5‰ lower than the measured $\delta^{15}N_{NO3}$ ($\delta^{15}N_{PON}$ of ∼7‰, $\delta^{15}N_{NO3}$ of ∼12‰; Figure 3). The $\delta^{15}N_{PON}$ is set by the $\delta^{15}N$ of the assimilated N sources and by the extent of their consumption (Fawcett et al., 2011, 2014; Treibergs et al., 2014). Given an isotope effect for NO_3^- assimilation of ∼5‰ (e.g., Fripiat et al., 2019; Granger et al., 2004, 2010; Wada & Hattori, 1978), our data suggest that the main N source used by nanoplankton was NO_3^- since its consumption would yield PON with a $\delta^{15}N$ that was ∼5‰ lower than the $\delta^{15}N_{NO3}$, as was observed. In the surface layer of the ocean, NH_4^+ is generally low in $\delta^{15}N$ (<0‰) because of isotope fractionation associated with the metabolic processes that result in its production (Checkley & Miller, 1989). At the same time, the isotope effect of NH_4^+ assimilation appears to be near-zero when NH_4^+ concentrations are <5 μM (Liu et al., 2013; Pennock et al., 1996). Thus, if phytoplankton were relying predominantly on NH_4^+ to fuel production, we should have

observed lower values of $\delta^{15}N_{PON,}$ which was not the case. We thus conclude that the nanoplankton $\delta^{15}N_{PON}$ data indicate sustained reliance by this size class on NO_3^-.

While we have almost no reliable microplankton $\delta^{15}N_{PON}$ data, the picoplankton $\delta^{15}N_{PON}$ was relatively high at the surface pre-upwelling and at depth post-upwelling, reaching 15‰ (Figure 3g). A likely explanation for the deeper picoplankton $\delta^{15}N_{PON}$ is that this group consumed NH_4^+ that was high in $\delta^{15}N$. The partial nitrification of subsurface NH_4^+, which occurs with a large isotope effect (14–19‰; Casciotti et al., 2003), generates residual NH_4^+ that can be very high in $\delta^{15}N$. The assimilation of this NH_4^+ by picoplankton would cause their $\delta^{15}N_{PON}$ to be similarly high since NH_4^+ assimilation occurs without isotopic fractionation (Liu et al., 2013). We note, however, that the picoplankton PON concentrations were generally very low, often falling below the methodological detention limit, such that their $\delta^{15}N_{PON}$ should be interpreted with caution. Regardless, our data strongly suggest very different nutrient acquisition strategies for nanoplankton versus picoplankton, which presumably contribute to their relative abundance and success in the SBUS (Burger et al., 2020).

4.2. LC Omega-3 Production in the SBUS

As for most of the parameters investigated, TFA and LC omega-3 concentrations were higher pre- and post-upwelling at 0 and 5 m, decreasing to near-zero at depth and during upwelling (Figure 6), except in the case of bottom-water samples collected on days 4, 5, and 10 (see below). Since LC omega-3 in the ocean are largely produced by phytoplankton (e.g., Dalsgaard et al., 2003), we expected to find them in the euphotic zone during periods of relaxation characterized by enhanced diatom productivity. The extremely high LC omega-3 concentrations recorded pre-upwelling were nonetheless unexpected. Indeed, this study revealed two novel findings regarding LC omega-3: (a) the speed with which the phytoplankton community changed from pre- to post-upwelling and the (related) rapid production of FA and LC omega-3 post-upwelling, and (b) the high concentrations of FA and LC omega-3 associated with SBUS phytoplankton. We discuss each of these findings below.

Phytoplankton community composition rapidly changed over the upwelling cycle, and the TFA and LC omega-3 concentrations returned to pre-upwelling levels within just 2 days of the upwelling event. All FA analyses indicate a clear separation among samples collected pre-, during, and post-upwelling. The pre-upwelling community was mostly characterized by non-diatom TM, including haptophyte and dinoflagellate TM (together >50% of TFA), while the post-upwelling assemblage was dominated by diatom TM (>60% of TFA) (Figure 6 and Figure S7 in Supporting Information S1). During upwelling, no dominant TM was identified. It is well known that phytoplankton community composition is the main factor driving variability in FA profiles (Galloway & Winder, 2015). Diatoms are usually the first phytoplankton group to proliferate post-upwelling as they are NO_3^- specialists that respond rapidly to an input of new nutrients (Fawcett & Ward, 2011; Kudela & Dugdale, 2000; Van Oostende et al., 2015) and are able to cope under variable light conditions (Guerrero et al., 1981; Syrett, 1981). The diatom bloom is generally succeeded by dinoflagellates, typically once the micronutrient and macronutrient essential for diatom production are depleted (Martin-Jézéquel et al., 2000; Tilstone et al., 2000). Additionally some dinoflagellates in the SBUS are mixotrophs, such that they can proliferate under the reduced nutrient conditions typical of post-upwelling (e.g., Pitcher, 2008; van der Lingen et al., 2016).

This work was conducted during the SBUS upwelling season, where upwelling "cycles" (i.e., upwelling followed by relaxation) typically last 3–10 days (Nelson & Hutchings, 1983). The high non-diatom TM recorded pre-upwelling could be linked to the post-diatom bloom community associated with a previous upwelling event. Diatom TM were also present pre-upwelling, albeit at lower concentrations than the non-diatom TM (20% versus 50% of TFA), even though the microscopy data suggest that large diatoms (>50 μm) were not abundant pre-upwelling. The diatom *Chaetoceros* spp. was the main type of phytoplankton identified by microscopy and was present in extremely high numbers post-upwelling (Figure 4). Since this species can occur in both chains and as single cells (Stoermer & Julius, 2003), it could also have been present in relatively high abundances pre-upwelling but not represented in the microscopy samples. While the succession of diatoms by dinoflagellates is frequently observed in upwelling systems (Hansen et al., 2014; Pitcher et al., 1991; Puccinelli, McQuaid, et al., 2016), the speed with which the FA content of the community changed (i.e., from TFA of 131.4 μg L^{-1} on day 4 to ~0 on day 6 and then to 109.8 μg L^{-1} on day 8) is nonetheless remarkable. Our data suggest that both diatoms and non-diatoms produce large amounts of LC omega-3 in Elandsbaai. The EPA produced by diatoms and the DHA produced by haptophytes and dinoflagellates (Dalsgaard et al., 2003; Remize et al., 2020) are the two most important LC omega-3 in the ocean, essential for higher trophic levels including humans (Hicks et al., 2019; Tocher et al., 2019).

The second novel finding of this work is the extremely high concentrations of FA and LC omega-3 observed for SBUS phytoplankton. The information available on LC omega-3 production for the BUS (NBUS + SBUS) is limited (Puccinelli et al., 2021), with the only published data being the LC omega-3 content of suspended organic matter (1–5 μg L^{-1}) collected from a rocky shore environment in the SBUS (Puccinelli, McQuaid, et al., 2016; Puccinelli, Noyon, et al., 2016). Here, we report TFA concentrations of up to 215.5 and 175.3 μg L^{-1} and LC omega-3 of up to 49.3 and 44.5 μg L^{-1} pre- and post-upwelling, respectively (Figure 6). That is, we measured LC omega-3 concentrations that are 10 times higher than previously reported for the SBUS. The discrepancy between our measurements of those reported in the earlier SBUS study may be due to sampling location, with Puccinelli, McQuaid, et al. (2016) focused on a rocky shore environment, in contrast to the open water site investigated here. In Elandsbaai, elevated mixing during upwelling that supplied nutrients to the surface layer favored high LC omega-3 production by phytoplankton immediately following upwelling, an effect that is likely limited in nearshore/rocky shore regions.

The magnitude of the discrepancy between the two SBUS studies is nonetheless very large. The concentrations of TFA and LC omega-3 measured in this study are also higher than those observed in other EBUS, with TFA of 50–70 and 2–70 μg L^{-1} and LC omega-3 of 8–11 and 1–18 μg L^{-1} reported for the California and Humboldt upwelling systems, respectively (Fischer et al., 2014; Gutiérrez et al., 2012), while no information is available for the Canary system (Puccinelli et al., 2021). Among the studies investigating LC omega-3 production by phytoplankton in EBUS, ours is the first to account for temporal variability and/or to investigate the effect(s) of the upwelling cycle. Snapshot samplings will record LC omega-3 production under specific conditions only (i.e., partway through the upwelling or relaxation phase), which may partly explain the apparent inconsistency with our work. For instance, if sampling were conducted on a day of active upwelling only, we would have recorded LC omega-3 concentrations close to 0 μg L^{-1}. This value is orders of magnitude lower than the concentrations we measured during the relaxation periods, such that if it were taken as broadly representative of our system, it would have led us to strongly underestimate LC omega-3 production. We thus suggest that LC omega-3 production in the SBUS, and in upwelling systems more broadly, has previously been considerably underestimated, likely due to sampling limitations. In fact, available studies focusing on LC omega-3 in upwelling regions have limited spatial, temporal, and/or depth resolution (e.g., Fischer et al., 2014; Gutiérrez et al., 2012; Puccinelli, McQuaid, et al., 2016; Puccinelli, Noyon, et al., 2016).

The NQI, which quantifies the nutritional value of phytoplankton communities based on FA (Cañavate, 2019), was in the range of 216.5 ± 15.3 pre- and post-upwelling, but decreased at depth and during upwelling (89.7 ± 13.5). The highest NQIs derived here are similar to those reported for other reach ocean basins (e.g., Mayzaud et al., 2007; Nichols et al., 1991; Remize et al., 2022). The relatively high NQIs computed for Elandsbaai can be ascribed to the phytoplankton groups that dominated pre- and post-upwelling (haptophytes/dinoflagellates and diatoms, respectively), which are the main producers of the nutritious DHA and EPA (Cañavate, 2019; Galloway & Winder, 2015). Our results indicate that the production of both types of LC omega-3 was responsible for the high NQIs, indicating that this phytoplankton constitutes a highly nutritious food source for higher trophic levels. In contrast, NQIs at depth (>10 m) and during upwelling were generally low, likely linked to the low abundance of phytoplankton, which reduced LC omega-3 concentrations and in turn the NQIs. Additionally, LC omega-3 can easily degrade with depth or be consumed (Budge et al., 2006; Conte et al., 1995), which will reduce the nutritional value of LC omega-3.

The high TFA and LC omega-3 concentrations, and NQI, observed at depth on days 4, 5, and 10 (Figure 6) could be linked to phytoplankton sinking (i.e., organic matter export) and/or the formation of phytoplankton resting spores at the sediment-water interface (Pitcher, 1986; Pitcher et al., 1991). These processes may represent an important mechanism supplying FA to the benthos in Elandsbaai, including to the commercially relevant rock lobster, an important fishery on South Africa's west coast (Bailey & Chapman, 1991). While this study did not focus on the benthos, our results suggest that the effects of upwelling on FA production may extend to benthic communities, with further studies needed to clarify the connections and implications.

5. Implications for Future LC Omega-3 Availability

The work detailed here highlights the key role that upwelling plays in promoting the success of a phytoplankton community in the SBUS that produces elevated concentrations of high-quality LC omega-3. This study also shows the remarkable speed of the phytoplankton response to upwelling-driven changes to the SBUS water

column, with the community then returning to a pre-upwelling state within 2 to 3 days of an upwelling event. We found that the SBUS phytoplankton community, which relied largely on NO_3^- supplied to the surface layer by upwelling, produced concentrations of LC omega-3 that were considerably higher than the current estimates available for any of the EBUS, implicating a tight link between new NO_3^- consumption and LC omega-3 production. Since phytoplankton form the base of the food web and are the main producers of LC omega-3 in the ocean, investigating the relationship of LC omega-3 concentrations to phytoplankton production with depth and time provides a way of evaluating the amount of LC omega-3 available in the system at present and in the future.

Current LC omega-3 production estimates, based mainly on meta analyses and laboratory/mesocosm experiments, suggest that the global LC omega-3 supply may soon become insufficient for a growing human population (Colombo et al., 2020; Hamilton et al., 2020; Hixson & Arts, 2016), which is predicted to reach 11 billion by 2100 (Roser, 2013) (noting that these estimates do not account for other factors that may affect the supply to humans, such us overfishing; Shepon et al., 2022). The results of our study indicate that the LC omega-3 supply is not as limited as previously surmised, as we measured LC omega-3 concentrations that were 10 times higher than earlier estimates from the SBUS. Indeed, our new concentration data for the SBUS, combined with the general lack of information available on LC omega-3 production in upwelling systems, suggest that global LC omega-3 production may be significantly underestimated. Similar high-resolution (temporal and spatial) studies are needed to better quantify the stock of LC omega-3 available for higher trophic levels (including humans) across the global ocean.

Conflict of Interest

The authors declare no conflicts of interest relevant to this study.

Data Availability Statement

The authors declare that all data relative to this work are included in the manuscript in the form of tables or Supporting Information S1. These data are also available in a public open access repository with the DOI: https://doi.org/10.25850/nioz/7b.b.kf as part of the Data Archive System (DAS) of NIOZ.

Acknowledgments
This work was supported by the ISblue project, Interdisciplinary graduate school for the blue planet (ANR-17-EURE-0015), cofunded by the French government under the program "Investissements d'Avenir" and SAD programme fellowship to EP. Additional funding was provided by the South African National Research Foundation (115335, 116142, 129320), the University of Cape Town (UCT) Research Committee, and a Royal Society/African Academy of Sciences Future Leaders Africa Independent Researcher (FLAIR) fellowship to SF. We acknowledge the LIPIDOCEAN and the Plateforme Isotope Stable du Pôle Spectrométrie Océan (PSO) at the Institut Universitaire Européen de la Mer (Plouzané, France), the Marine Biogeochemistry Lab and the Stable Light Isotope Laboratory at UCT, the UC Davis Stable Isotope Facility, the South African Weather Service (SAWS), and the South African Department of Science and Innovation's Biogeochemistry Research Infrastructure Platform (BIOGRIP). We are grateful to Pieter Truter and the Research Dive Unit at UCT for their assistance at sea, and to members of the Fawcett research group for their help with sample collection. The sea surface temperature data used in Figure 1 were obtained through the online Regional Air-Sear Interactions (RASI) tool at the NASA Global Hydrometeorology Resource Center DAAC, Huntsville, AL. https://opendap.earthdata.nasa.gov/collections/C2036881720-POCLOUD/granules/20200310120000-CMC-L4_GHRSST-SSTfnd-CMC0.1deg-GLOB-v02.0-fv03.0.

References

Anderson, M., Gorley, R., & Clarke, K. (2008). *PERMANOVA + for PRIMER: Guide to software and statistical methods*. PRIMER-E.

Archer, D. E., & Johnson, K. (2000). A model of the iron cycle in the ocean. *Global Biogeochemical Cycles*, *14*(1), 269–279. https://doi.org/10.1029/1999GB900053

Aristizábal, M. F., Fewings, M. R., & Washburn, L. (2017). Effects of the relaxation of upwelling-favorable winds on the diurnal and semidiurnal water temperature fluctuations in the Santa Barbara Channel, California. *Journal of Geophysical Research: Oceans*, *122*, 7958–7977. https://doi.org/10.1002/2017JC013199

Arts, M. T., Ackman, R. G., & Holub, B. J. (2001). "Essential fatty acids" in aquatic ecosystems: A crucial link between diet and human health and evolution. *Canadian Journal of Fisheries and Aquatic Sciences*, *58*(1), 122–137. https://doi.org/10.1139/f00-224

Bailey, G. W. (1991). Organic carbon flux and development of oxygen deficiency on the modern Benguela continental shelf south of 22°S: Spatial and temporal variability. *Geological Society, London, Special Publications*, *58*(1), 171–183. https://doi.org/10.1144/GSL.SP.1991.058.01.12

Bailey, G. W., & Chapman, P. (1991). Short-term variability during an anchor station study in the southern Benguela upwelling system: Chemical and physical oceanography. *Progress in Oceanography*, *28*(1), 9–37. https://doi.org/10.1016/0079-6611(91)90019-I

Bode, A., Botas, J. A., & Fernández, E. (1997). Nitrate storage by phytoplankton in a coastal upwelling environment. *Marine Biology*, *129*(3), 399–406. https://doi.org/10.1007/s002270050180

Böhlke, J. K., Mroczkowski, S. J., & Coplen, T. B. (2003). Oxygen isotopes in nitrate: New reference materials for $^{18}O:^{17}O:^{16}O$ measurements and observations on nitrate-water equilibration. *Rapid Communications in Mass Spectrometry*, *17*(16), 1835–1846. https://doi.org/10.1002/rcm.1123

Boshers, D. S., Granger, J., Tobias, C. R., Böhlke, J. K., & Smith, R. L. (2019). Constraining the oxygen isotopic composition of nitrate produced by nitrification. *Environmental Science & Technology*, *53*(3), 1206–1216. https://doi.org/10.1021/acs.est.8b03386

Bouvier, T., Troussellier, M., Anzil, A., Courties, C., & Servais, P. (2001). Using light scatter signal to estimate bacterial biovolume by flow cytometry. *Cytometry*, *44*(3), 188–194. https://doi.org/10.1002/1097-0320(20010701)44:3<188::AID-CYTO1111>3.0.CO;2-C

Buchwald, C., Santoro, A. E., McIlvin, M. R., & Casciotti, K. L. (2012). Oxygen isotopic composition of nitrate and nitrite produced by nitrifying cocultures and natural marine assemblages. *Limnology & Oceanography*, *57*(5), 1361–1375. https://doi.org/10.4319/lo.2012.57.5.1361

Budge, S. M., Iverson, S. J., & Koopman, H. N. (2006). Studying trophic ecology in marine ecosystems using fatty acids: A primer on analysis and interpretation. *Marine Mammal Science*, *22*(4), 759–801. https://doi.org/10.1111/j.1748-7692.2006.00079.x

Burger, J. M., Moloney, C. L., Walker, D. R., Parrott, R. G., & Fawcett, S. E. (2020). Drivers of short-term variability in phytoplankton production in an embayment of the southern Benguela upwelling system. *Journal of Marine Systems*, *208*, 103341. https://doi.org/10.1016/j.jmarsys.2020.103341

Cañavate, J. P. (2019). Advancing assessment of marine phytoplankton community structure and nutritional value from fatty acid profiles of cultured microalgae. *Reviews in Aquaculture*, *11*(3), 527–549. https://doi.org/10.1111/raq.12244

Carpenter, J. H. (1965). The accuracy of the Winkler method for dissolved oxygen Analysis1. *Limnology & Oceanography*, *10*(1), 135–140. https://doi.org/10.4319/lo.1965.10.1.0135

Casciotti, K. L., Sigman, D. M., Hastings, M. G., Böhlke, J. K., & Hilkert, A. (2002). Measurement of the oxygen isotopic composition of nitrate in seawater and freshwater using the denitrifier method. *Analytical Chemistry*, *74*(19), 4905–4912. https://doi.org/10.1021/ac020113w

Casciotti, K. L., Sigman, D. M., & Ward, B. B. (2003). Linking diversity and stable isotope fractionation in ammonia-oxidizing bacteria. *Geomicrobiology Journal*, *20*(4), 335–353. https://doi.org/10.1080/01490450303895

Checkley, D. M., & Miller, C. A. (1989). Nitrogen isotope fractionation by oceanic zooplankton. *Deep-Sea Research, Part A: Oceanographic Research Papers*, *36*(10), 1449–1456. https://doi.org/10.1016/0198-0149(89)90050-2

Colombo, S. M., Rodgers, T. F. M., Diamond, M. L., Bazinet, R. P., & Arts, M. T. (2020). Projected declines in global DHA availability for human consumption as a result of global warming. *Ambio*, *49*(4), 865–880. https://doi.org/10.1007/s13280-019-01234-6

Conte, M. H., Eglinton, G., Madreira, L. A. S., Rabouille, C., Labeyrie, L., Mudge, S., et al. (1995). Origin and fate of organic biomarker compounds in the water column and sediments of the eastern North Atlantic. *Philosophical Transactions of the Royal Society of London. Series B: Biological Sciences*, *348*(1324), 169–178. https://doi.org/10.1098/rstb.1995.0059

Cury, P., & Roy, C. (1989). Optimal environmental window and pelagic fish recruitment success in upwelling areas. *Canadian Journal of Fisheries and Aquatic Sciences*, *46*(4), 670–680. https://doi.org/10.1139/f89-086

Dalsgaard, J., St. John, M., Kattner, G., Müller-Navarra, D., & Hagen, W. (2003). Fatty acid trophic markers in the pelagic marine environment. *Advances in Marine Biology*, *46*, 225–340. https://doi.org/10.1016/s0065-2881(03)46005-7

de Boyer Montégut, C., Madec, G., Fischer, A. S., Lazar, A., & Iudicone, D. (2004). Mixed layer depth over the global ocean: An examination of profile data and a profile-based climatology. *Journal of Geophysical Research*, *109*, C12003. https://doi.org/10.1029/2004JC002378

Diamond, D. (1994). *QuikChem method 10-114-21-1-B: Silicate byflow injection analysis*. Lachat Instruments.

Dortch, Q. (1990). The interaction between ammonium and nitrate uptake in phytoplankton. *Marine Ecology Progress Series*, *61*(1), 183–201. https://doi.org/10.3354/meps061183

Dugdale, R. C., & Goering, J. J. (1967). Uptake of new and regenerated forms of nitrogen in primary productivity. *Limnology & Oceanography*, *12*(2), 196–206. https://doi.org/10.4319/lo.1967.12.2.0196

Dugdale, R. C., & Wilkerson, F. P. (1986). The use of ^{15}N to measure nitrogen uptake in eutrophic oceans; experimental considerations[1,2]. *Limnology & Oceanography*, *31*(4), 673–689. https://doi.org/10.4319/lo.1986.31.4.0673

Dugdale, R. C., Wilkerson, F. P., Hogue, V. E., & Marchi, A. (2006). Nutrient controls on new production in the Bodega Bay, California, coastal upwelling plume. *Deep Sea Research Part II: Topical Studies in Oceanography*, *53*(25), 3049–3062. https://doi.org/10.1016/j.dsr2.2006.07.009

Fawcett, S. E., Lomas, M. W., Casey, J. R., Ward, B. B., & Sigman, D. M. (2011). Assimilation of upwelled nitrate by small eukaryotes in the Sargasso Sea. *Nature Geoscience*, *4*(10), 717–722. https://doi.org/10.1038/ngeo1265

Fawcett, S. E., Lomas, M. W., Ward, B. B., & Sigman, D. M. (2014). The counterintuitive effect of summer-to-fall mixed layer deepening on eukaryotic new production in the Sargasso Sea. *Global Biogeochemical Cycles*, *28*, 86–102. https://doi.org/10.1002/2013GB004579

Fawcett, S. E., & Ward, B. B. (2011). Phytoplankton succession and nitrogen utilization during the development of an upwelling bloom. *Marine Ecology Progress Series*, *428*, 13–31. https://doi.org/10.3354/meps09070

Fawcett, S. E., Ward, B. B., Lomas, M. W., & Sigman, D. M. (2015). Vertical decoupling of nitrate assimilation and nitrification in the Sargasso Sea. *Deep Sea Research Part I: Oceanographic Research Papers*, *103*, 64–72. https://doi.org/10.1016/j.dsr.2015.05.004

Finkel, Z. V. (2001). Light absorption and size scaling of light-limited metabolism in marine diatoms. *Limnology & Oceanography*, *46*(1), 86–94. https://doi.org/10.4319/lo.2001.46.1.0086

Fischer, A. M., Ryan, J. P., Levesque, C., & Welschmeyer, N. (2014). Characterizing estuarine plume discharge into the coastal ocean using fatty acid biomarkers and pigment analysis. *Marine Environmental Research*, *99*, 106–116. https://doi.org/10.1016/j.marenvres.2014.04.006

Flynn, R. F., Granger, J., Veitch, J. A., Siedlecki, S., Burger, J. M., Pillay, K., & Fawcett, S. E. (2020). On-shelf nutrient trapping enhances the fertility of the southern Benguela upwelling system. *Journal of Geophysical Research: Oceans*, *125*, e2019JC015948. https://doi.org/10.1029/2019JC015948

Folch, J., Lees, M., & Sloane Stanley, G. H. (1957). A simple method for the isolation and purification of total lipides from animal tissues. *Journal of Biological Chemistry*, *226*(1), 497–509. https://doi.org/10.1016/s0021-9258(18)64849-5

Fripiat, F., Martínez-García, A., Fawcett, S. E., Kemeny, P. C., Studer, A. S., Smart, S. M., et al. (2019). The isotope effect of nitrate assimilation in the Antarctic Zone: Improved estimates and paleoceanographic implications. *Geochimica et Cosmochimica Acta*, *247*, 261–279. https://doi.org/10.1016/j.gca.2018.12.003

Galloway, A. W. E., & Winder, M. (2015). Partitioning the relative importance of phylogeny and environmental conditions on phytoplankton fatty acids. *PLoS One*, *10*(6), e0130053. https://doi.org/10.1371/journal.pone.0130053

Garrido, S., Rosa, R., Ben-Hamadou, R., Cunha, M. E., Chícharo, M. A., & van der Lingen, C. D. (2007). Effect of maternal fat reserves on the fatty acid composition of sardine (*Sardina pilchardus*) oocytes. *Comparative Biochemistry and Physiology Part B: Biochemistry and Molecular Biology*, *148*(4), 398–409. https://doi.org/10.1016/j.cbpb.2007.07.008

Glover, H. E., Garside, C., & Trees, C. C. (2007). Physiological responses of Sargasso Sea picoplankton to nanomolar nitrate perturbations. *Journal of Plankton Research*, *29*(3), 263–274. https://doi.org/10.1093/plankt/fbm013

Gonfiantini, R., Stichler, W., & Rozanski, K. (1995). Standards and intercomparison materials distributed by the International Atomic Energy Agency for stable isotope measurements. Retrieved from http://inis.iaea.org/Search/search.aspx?orig_q=RN:27021328

González-Galisteo, S., Packard, T. T., Gómez, M., Herrera, A., Dugdale, R. C., Wilkerson, F. P., et al. (2019). Calculating new production from nitrate reductase activity and light in the Peru current upwelling. *Progress in Oceanography*, *173*, 78–85. https://doi.org/10.1016/j.pocean.2019.02.009

Granger, J., Prokopenko, M. G., Sigman, D. M., Mordy, C. W., Morse, Z. M., Morales, L. V., et al. (2011). Coupled nitrification-denitrification in sediment of the eastern Bering Sea shelf leads to ^{15}N enrichment of fixed N in shelf waters. *Journal of Geophysical Research*, *116*, C11006. https://doi.org/10.1029/2010JC006751

Granger, J., & Sigman, D. M. (2009). Removal of nitrite with sulfamic acid for nitrate N and O isotope analysis with the denitrifier method. *Rapid Communications in Mass Spectrometry*, *23*(23), 3753–3762. https://doi.org/10.1002/rcm.4307

Granger, J., Sigman, D. M., Needoba, J. A., & Harrison, P. J. (2004). Coupled nitrogen and oxygen isotope fractionation of nitrate during assimilation by cultures of marine phytoplankton. *Limnology & Oceanography*, *49*(5), 1763–1773. https://doi.org/10.4319/lo.2004.49.5.1763

Granger, J., Sigman, D. M., Rohde, M. M., Maldonado, M. T., & Tortell, P. D. (2010). N and O isotope effects during nitrate assimilation by unicellular prokaryotic and eukaryotic plankton cultures. *Geochimica et Cosmochimica Acta*, *74*(3), 1030–1040. https://doi.org/10.1016/j.gca.2009.10.044

Grasshoff, K. (1976). *Methods of seawater analysis*. Verlag Chemie, Weinheim.

Guerrero, M. G., Vega, J. M., & Losada, M. (1981). The assimilatory nitrate-Reducing system and its regulation. *Annual Review of Plant Physiology*, *32*(1), 169–204. https://doi.org/10.1146/annurev.pp.32.060181.001125

Gutiérrez, M. H., Pantoja, S., & Lange, C. B. (2012). Biogeochemical significance of fatty acid distribution in the coastal upwelling ecosystem off Concepción (36°S), Chile. *Organic Geochemistry*, *49*, 56–67. https://doi.org/10.1016/j.orggeochem.2012.05.010

Hamilton, H. A., Newton, R., Auchterlonie, N. A., & Müller, D. B. (2020). Systems approach to quantify the global omega-3 fatty acid cycle. *Nature Food*, *1*(1), 59–62. https://doi.org/10.1038/s43016-019-0006-0

Hansen, A., Ohde, T., & Wasmund, N. (2014). Succession of micro- and nanoplankton groups in ageing upwelled waters off Namibia. *Journal of Marine Systems*, *140*, 130–137. https://doi.org/10.1016/j.jmarsys.2014.05.003

Hicks, C. C., Cohen, P. J., Graham, N. A. J., Nash, K. L., Allison, E. H., D'Lima, C., et al. (2019). Harnessing global fisheries to tackle micronutrient deficiencies. *Nature*, *574*(7776), 95–98. https://doi.org/10.1038/s41586-019-1592-6

Hixson, S. M., & Arts, M. T. (2016). Climate warming is predicted to reduce omega-3, long-chain, polyunsaturated fatty acid production in phytoplankton. *Global Change Biology*, *22*(8), 2744–2755. https://doi.org/10.1111/gcb.13295

Holmes, R. M., Aminot, A., Kérouel, R., Hooker, B. A., & Peterson, B. J. (1999). A simple and precise method for measuring ammonium in marine and freshwater ecosystems. *Canadian Journal of Fisheries and Aquatic Sciences*, *56*(10), 1801–1808. https://doi.org/10.1139/f99-128

Huggett, J., Verheye, H., Escribano, R., & Fairweather, T. (2009). Copepod biomass, size composition and production in the Southern Benguela: Spatio-temporal patterns of variation, and comparison with other eastern boundary upwelling systems. *Progress in Oceanography*, *83*(1), 197–207. https://doi.org/10.1016/j.pocean.2009.07.048

Hutchings, L., van der Lingen, C. D., Shannon, L. J., Crawford, R. J. M., Verheye, H. M. S., Bartholomae, C. H., et al. (2009). The Benguela Current: An ecosystem of four components. *Progress in Oceanography*, *83*(1), 15–32. https://doi.org/10.1016/j.pocean.2009.07.046

Idso, S. B., & Gilbert, R. G. (1974). On the universality of the Poole and Atkins Secchi disk-light extinction equation. *Journal of Applied Ecology*, *11*(1), 399–401. https://doi.org/10.2307/2402029

IOC. (2010). Intergovernmental Oceanographic Commission. *The International thermodynamic equation of seawater–2010: Calculation and use of thermodynamic properties*. Retrieved from http://www.teos-10.org/pubs/TEOS-10_Manual.pdf. UNESCO. Retrieved from https://unesdoc.unesco.org/ark:/48223/pf0000188170

Jónasdóttir, S. H. (2019). Fatty acid profiles and production in marine phytoplankton. *Marine Drugs*, *17*(3), 151. https://doi.org/10.3390/md17030151

Kirk, J. T. O. (1994). *Light and photosynthesis in aquatic ecosystems* (2nd ed.). Cambridge University Press. https://doi.org/10.1017/CBO9780511623370

Kudela, R. M., & Dugdale, R. C. (2000). Nutrient regulation of phytoplankton productivity in Monterey Bay, California. *Deep Sea Research Part II: Topical Studies in Oceanography*, *47*(5), 1023–1053. https://doi.org/10.1016/S0967-0645(99)00135-6

Lamont, T., Hutchings, L., van den Berg, M. A., Goschen, W. S., & Barlow, R. G. (2015). Hydrographic variability in the St. Helena Bay region of the southern Benguela ecosystem. *Journal of Geophysical Research: Oceans*, *120*, 2920–2944. https://doi.org/10.1002/2014JC010619

Litchman, E. (2007). Chapter 16—Resource competition and the ecological success of phytoplankton. In P. G. Falkowski, & A. H. Knoll (Eds.), *Evolution of primary producers in the sea* (pp. 351–375). Academic Press. https://doi.org/10.1016/B978-012370518-1/50017-5

Litzow, M. A., Bailey, K. M., Prahl, F. G., & Heintz, R. (2006). Climate regime shifts and reorganization of fish communities: The essential fatty acid limitation hypothesis. *Marine Ecology Progress Series*, *315*, 1–11. https://doi.org/10.3354/meps315001

Liu, K.-K., Kao, S.-J., Chiang, K.-P., Gong, G.-C., Chang, J., Cheng, J.-S., & Lan, C.-Y. (2013). Concentration dependent nitrogen isotope fractionation during ammonium uptake by phytoplankton under an algal bloom condition in the Danshuei estuary, northern Taiwan. *Marine Chemistry*, *157*, 242–252. https://doi.org/10.1016/j.marchem.2013.10.005

Mariotti, A., Germon, J. C., Hubert, P., Kaiser, P., Letolle, R., Tardieux, A., & Tardieux, P. (1981). Experimental determination of nitrogen kinetic isotope fractionation: Some principles; illustration for the denitrification and nitrification processes. *Plant and Soil*, *62*(3), 413–430. https://doi.org/10.1007/BF02374138

Martin-Jézéquel, V., Hildebrand, M., & Brzezinski, M. A. (2000). Silicon metabolism in diatoms: Implications for growth. *Journal of Phycology*, *36*(5), 821–840. https://doi.org/10.1046/j.1529-8817.2000.00019.x

Mayzaud, P., Laureillard, J., Merien, D., Brinis, A., Godard, C., Razouls, S., & Labat, J.-P. (2007). Zooplankton nutrition, storage and fecal lipid composition in different water masses associated with the Agulhas and Subtropical Fronts. *Marine Chemistry*, *107*(2), 202–213. https://doi.org/10.1016/j.marchem.2007.07.001

Messié, M., & Chavez, F. P. (2015). Seasonal regulation of primary production in eastern boundary upwelling systems. *Progress in Oceanography*, *134*, 1–18. https://doi.org/10.1016/j.pocean.2014.10.011

Messié, M., Ledesma, J., Kolber, D. D., Michisaki, R. P., Foley, D. G., & Chavez, F. P. (2009). Potential new production estimates in four eastern boundary upwelling ecosystems. *Progress in Oceanography*, *83*(1), 151–158. https://doi.org/10.1016/j.pocean.2009.07.018

Monteiro, P. M. S., Dewitte, B., Scranton, M. I., Paulmier, A., & van der Plas, A. K. (2011). The role of open ocean boundary forcing on seasonal to decadal-scale variability and long-term change of natural shelf hypoxia. *Environmental Research Letters*, *6*(2), 025002. https://doi.org/10.1088/1748-9326/6/2/025002

Mourente, G. (2003). Accumulation of DHA (docosahexaenoic acid; 22:6n-3). In *Larval and juvenile fish brain*. Bergen.

Nelson, G., & Hutchings, L. (1983). The Benguela upwelling area. *Progress in Oceanography*, *12*(3), 333–356. https://doi.org/10.1016/0079-6611(83)90013-7

Nichols, P. D., Skerratt, J. H., Davidson, A., Burton, H., & Mcmeekin, T. A. (1991). Lipids of cultured *Phaeocystis pouchetii*: Signatures for food-web, biogeochemical and environmental studies in Antarctica and the Southern Ocean. *Phytochemistry*, *30*(10), 3209–3214. https://doi.org/10.1016/0031-9422(91)83177-M

Parrish, C. C. (2013). *Lipids in marine ecosystems* [Review Article]. Hindawi Publishing Corporation. https://doi.org/10.5402/2013/604045

Parrish, C. C., Abrajano, T. A., Budge, S. M., Helleur, R. J., Hudson, E. D., Pulchan, K., & Ramos, C. (2000). Lipid and phenolic biomarkers in marine ecosystems: Analysis and applications. In P. J. Wangersky (Ed.), *Marine chemistry* (pp. 193–223). Springer Berlin Heidelberg. Retrieved from http://link.springer.com/chapter/10.1007/10683826_8

Parsons, T. R., Maita, Y., & Lalli, C. M. (1984). *A manual of chemical & biological methods for seawater analysis*. Elsevier. https://doi.org/10.1016/C2009-0-07774-5

Patti, B., Guisande, C., Vergara, A. R., Riveiro, I., Maneiro, I., Barreiro, A., et al. (2008). Factors responsible for the differences in satellite-based chlorophyll *a* concentration between the major global upwelling areas. *Estuarine, Coastal and Shelf Science*, *76*(4), 775–786. https://doi.org/10.1016/j.ecss.2007.08.005

Pauly, D., & Christensen, V. (1995). Primary production required to sustain global fisheries. *Nature*, *374*(6519), 255–257. https://doi.org/10.1038/374255a0

Pennock, J. R., Velinsky, D. J., Ludlam, J. M., Sharp, J. H., & Fogel, M. L. (1996). Isotopic fractionation of ammonium and nitrate during uptake by *Skeletonema costatum*: Implications for $\delta^{15}N$ dynamics under bloom conditions. *Limnology & Oceanography*, *41*(3), 451–459. https://doi.org/10.4319/lo.1996.41.3.0451

Pitcher, G. C. (1986). Sedimentary flux and the formation of resting spores of selected *Chaetoceros* species at two sites in the southern Benguela System. *South African Journal of Marine Science*, *4*(1), 231–244. https://doi.org/10.2989/025776186784461657

Pitcher, G. C., Bernard, S., & Ntuli, J. (2008). Contrasting bays and red tides in the southern Benguela upwelling system. *Oceanography*, *21*(3), 82–91. https://doi.org/10.5670/oceanog.2008.39

Pitcher, G. C., & Calder, D. (2000). Harmful algal blooms of the southern Benguela current: A review and appraisal of monitoring from 1989 to 1997. *South African Journal of Marine Science*, *22*(1), 255–271. https://doi.org/10.2989/025776100784125681

Pitcher, G. C., Walker, D. R., Mitchell-Innes, B. A., & Moloney, C. L. (1991). Short-term variability during an anchor station study in the southern Benguela upwelling system: Phytoplankton dynamics. *Progress in Oceanography*, *28*(1–2), 39–64. https://doi.org/10.1016/0079-6611(91)90020-M

Probyn, T. A. (1992). The inorganic nitrogen nutrition of phytoplankton in the southern Benguela: New production, phytoplankton size and implications for pelagic foodwebs. *South African Journal of Marine Science*, *12*(1), 411–420. https://doi.org/10.2989/02577619209504715

Probyn, T. A., & Painting, S. J. (1985). Nitrogen uptake by size-fractionated phytoplankton populations in Antarctic surface waters. *Limnology & Oceanography*, *30*(6), 1327–1332. https://doi.org/10.4319/lo.1985.30.6.1327

Puccinelli, E., McQuaid, C. D., & Noyon, M. (2016). Spatio-temporal variation in effects of upwelling on the fatty acid composition of benthic filter feeders in the southern Benguela ecosystem: Not all upwelling is equal. *PLoS One*, *11*(8), e0161919. https://doi.org/10.1371/journal.pone.0161919

Puccinelli, E., Noyon, M., & McQuaid, C. (2016). Hierarchical effects of biogeography and upwelling shape the dietary signatures of benthic filter feeders. *Marine Ecology Progress Series*, *543*, 37–54. https://doi.org/10.3354/meps11567

Puccinelli, E., Sardenne, F., Pecquerie, L., Fawcett, S. E., Machu, E., & Soudant, P. (2021). Omega-3 pathways in upwelling systems: The link to nitrogen supply. *Frontiers in Marine Science*, *8*, 1–10. https://doi.org/10.3389/fmars.2021.664601

Ravet, J. L., Brett, M. T., & Arhonditsis, G. B. (2010). The effects of seston lipids on zooplankton fatty acid composition in Lake Washington, Washington, USA. *Ecology*, *91*(1), 180–190. https://doi.org/10.1890/08-2037.1

Remize, M., Planchon, F., Loh, A. N., Grand, F. L., Bideau, A., Goic, N. L., et al. (2020). Study of synthesis pathways of the essential polyunsaturated fatty acid 20:5n-3 in the diatom *Chaetoceros muelleri* using 13C-isotope labeling. *Biomolecules*, *10*(5), 797. https://doi.org/10.3390/biom10050797

Remize, M., Planchon, F., Loh, A. N., Le Grand, F., Bideau, A., Puccinelli, E., et al. (2022). Origin and fate of long-chain polyunsaturated fatty acids in the Kerguelen Islands region (Southern Ocean) in late summer. *Journal of Marine Systems*, *228*, 103693. https://doi.org/10.1016/j.jmarsys.2021.103693

Roser, M. (2013). Future population growth. *Our world in data*. Retrieved from https://ourworldindata.org/future-population-growth

Saxberg, B. E., & Kowalski, B. R. (1979). Generalized standard addition method. *Analytical Chemistry*, *51*(7), 1031–1038. https://doi.org/10.1021/ac50043a059

Shannon, L. (1985). The Benguela ecosystem. I: Evolution of the Benguela physical features and processes. *Undefined*. Retrieved from https://www.semanticscholar.org/paper/The-Benguela-ecosystem.-I%3A-Evolution-of-the-and-Shannon/264dec3872d80bea3a33909e1e8509c9b81d6dda

Shannon, L. V., & Nelson, G. (1996). The Benguela: Large scale features and processes and system variability. In *The South Atlantic* (pp. 163–210). Springer Berlin Heidelberg. Retrieved from http://link.springer.com/chapter/10.1007/978-3-642-80353-6_9

Shepon, A., Makov, T., Hamilton, H. A., Müller, D. B., Gephart, J. A., Henriksson, P. J. G., et al. (2022). Sustainable optimization of global aquatic omega-3 supply chain could substantially narrow the nutrient gap. *Resources, Conservation and Recycling*, *181*, 106260. https://doi.org/10.1016/j.resconrec.2022.106260

Sigman, D. M., Altabet, M. A., McCorkle, D. C., Francois, R., & Fischer, G. (1999). The $\delta^{15}N$ of nitrate in the Southern Ocean: Consumption of nitrate in surface waters. *Global Biogeochemical Cycles*, *13*(4), 1149–1166. https://doi.org/10.1029/1999GB900038

Sigman, D. M., Casciotti, K. L., Andreani, M., Barford, C., Galanter, M., & Böhlke, J. K. (2001). A bacterial method for the nitrogen isotopic analysis of nitrate in seawater and freshwater. *Analytical Chemistry*, *73*(17), 4145–4153. https://doi.org/10.1021/ac010088e

Sigman, D. M., DiFiore, P. J., Hain, M. P., Deutsch, C., Wang, Y., Karl, D. M., et al. (2009). The dual isotopes of deep nitrate as a constraint on the cycle and budget of oceanic fixed nitrogen. *Deep Sea Research Part I: Oceanographic Research Papers*, *56*(9), 1419–1439. https://doi.org/10.1016/j.dsr.2009.04.007

Stoermer, E. F., & Julius, M. L. (2003). 15-Centric diatoms. In J. D. Wehr, & R. G. Sheath (Eds.), *Freshwater algae of North America* (pp. 559–594). Academic Press. https://doi.org/10.1016/B978-012741550-5/50016-7

Syrett, J. P. (1981). Nitrogen metabolism of microalgae. *Canadian Bulletin of Fisheries and Aquatic Sciences*, *210*, 182–210.

Tacon, A. G. J., & Metian, M. (2009). Fishing for feed or fishing for food: Increasing global competition for small pelagic forage fish. *Ambio*, *38*(6), 294–302. https://doi.org/10.2307/40390239

Tilstone, G., Míguez, B., Figueiras, F., & Fermín, E. (2000). Diatom dynamics in a coastal ecosystem affected by upwelling: Coupling between species succession, circulation and biogeochemical processes. *Marine Ecology Progress Series*, *205*, 23–41. https://doi.org/10.3354/meps205023

Tocher, D. R. (2015). Omega-3 long-chain polyunsaturated fatty acids and aquaculture in perspective. *Aquaculture*, *449*, 94–107. https://doi.org/10.1016/j.aquaculture.2015.01.010

Tocher, D. R., Betancor, M. B., Sprague, M., Olsen, R. E., & Napier, J. A. (2019). Omega-3 long-chain polyunsaturated fatty acids, EPA and DHA: Bridging the gap between supply and Demand. *Nutrients*, *11*(1), 89. https://doi.org/10.3390/nu11010089

Treibergs, L. A., Fawcett, S. E., Lomas, M. W., & Sigman, D. M. (2014). Nitrogen isotopic response of prokaryotic and eukaryotic phytoplankton to nitrate availability in Sargasso Sea surface waters. *Limnology & Oceanography*, *59*(3), 972–985. https://doi.org/10.4319/lo.2014.59.3.0972

Tyrrell, T., & Lucas, M. I. (2002). Geochemical evidence of denitrification in the Benguela upwelling system. *Continental Shelf Research*, *22*(17), 2497–2511. https://doi.org/10.1016/S0278-4343(02)00077-8

van der Lingen, C. D., Hutchings, L., Lamont, T., & Pitcher, G. C. (2016). Climate change, dinoflagellate blooms and sardine in the southern Benguela current large marine ecosystem. *Environmental Development*, *17*, 230–243. https://doi.org/10.1016/j.envdev.2015.09.004

Van Oostende, N., Dunne, J. P., Fawcett, S. E., & Ward, B. B. (2015). Phytoplankton succession explains size-partitioning of new production following upwelling-induced blooms. *Journal of Marine Systems*, *148*, 14–25. https://doi.org/10.1016/j.jmarsys.2015.01.009

Veitch, J., Penven, P., & Shillington, F. (2010). Modeling equilibrium dynamics of the Benguela Current System. *Journal of Physical Oceanography*, *40*(9), 1942–1964. https://doi.org/10.1175/2010JPO4382.1

Wada, E., & Hattori, A. (1978). Nitrogen isotope effects in the assimilation of inorganic nitrogenous compounds by marine diatoms. *Geomicrobiology Journal*, *1*(1), 85–101. https://doi.org/10.1080/01490457809377725

Waldron, H. N., & Probyn, T. A. (1992). Nitrate supply and potential new production in the Benguela upwelling system. *South African Journal of Marine Science*, *12*(1), 29–39. https://doi.org/10.2989/02577619209504688

Ward, T. M., Mcleay, L. J., Dimmlich, W. F., Rogers, P. J., Mcclatchie, S., Matthews, R., et al. (2006). Pelagic ecology of a northern boundary current system: Effects of upwelling on the production and distribution of sardine (*Sardinops sagax*), anchovy (*Engraulis australis*) and southern bluefin tuna (*Thunnus maccoyii*) in the Great Australian Bight. *Fisheries Oceanography*, *15*(3), 191–207. https://doi.org/10.1111/j.1365-2419.2006.00353.x

Welschmeyer, N. A. (1994). Fluorometric analysis of chlorophyll *a* in the presence of chlorophyll b and pheopigments. *Limnology & Oceanography*, *39*(8), 1985–1992. https://doi.org/10.4319/lo.1994.39.8.1985

Zhang, Y., Bellingham, J. G., Ryan, J. P., & Godin, M. A. (2015). Evolution of a physical and biological front from upwelling to relaxation. *Continental Shelf Research*, *108*, 55–64. https://doi.org/10.1016/j.csr.2015.08.005